Effects of ice nuclei on cirrus clouds in a global climate model

J. Hendricks,[1] B. Kärcher,[1] and U. Lohmann[2]

Received 5 November 2010; revised 12 May 2011; accepted 9 June 2011; published 23 September 2011.

[1] A multiple-mode ice microphysical scheme is applied in the European Centre/Hamburg (ECHAM) general circulation model to simulate effects of aerosol-ice interactions on global cirrus properties. The different ice modes represent cirrus ice formed by homogeneous freezing of liquid aerosols and heterogeneous nucleation on mineral dust or black carbon particles. A fourth ice mode represents ice from other sources. The competition of these modes for available water is realized in a physical parameterization scheme considering also the effect of preexisting ice on the ice nucleation process. The model is applied to analyze the global characteristics of ice formed by the different aerosol types and to study potential global effects of mineral dust and black carbon particles on cirrus microphysical parameters. The simulations reveal that, on average, ice from heterogeneous nucleation shows fewer but larger crystals and has a smaller contribution to the mean cirrus ice water content than ice from homogeneous freezing. However, heterogeneous ice nuclei may have important effects on the overall cirrus properties. Reductions in zonal mean annual average cirrus ice particle number concentrations induced by heterogeneous nucleation of up to 20% in the tropics and 1%–10% in the midlatitudes are simulated. The effect is further amplified by ice formation on aircraft-generated soot. Significant reductions in the mean ice water content are modeled, which likely result from efficient sedimentation and precipitation of large ice particles generated by heterogeneous nucleation. This leads to reductions in the zonal mean annual average water vapor mixing ratio of up to 5% at cirrus levels.

Citation: Hendricks, J., B. Kärcher, and U. Lohmann (2011), Effects of ice nuclei on cirrus clouds in a global climate model, *J. Geophys. Res.*, *116*, D18206, doi:10.1029/2010JD015302.

1. Introduction

[2] The climatic effect of cloud perturbations due to anthropogenic aerosol changes, the aerosol indirect effect, is one of the key issues in climate research [e.g., *Forster et al.*, 2007; *Heintzenberg and Charlson*, 2009]. Many studies focus on interactions of aerosol with warm and mixed-phase clouds [*Lohmann and Feichter*, 2005]. The role of ice nucleating aerosol in cirrus cloud formation receives increasing attention [*Kärcher and Spichtinger*, 2009], partly triggered by new activities to study the aviation impact on climate change [*Lee et al.*, 2009; *Brasseur and Gupta*, 2010].

[3] Aerosol-induced cirrus formation occurs via two basic mechanisms. Ice particles form by homogeneous freezing of supercooled liquid solution particles [e.g., *Heymsfield and Sabin*, 1989; *Koop et al.*, 2000] or by heterogeneous ice nucleation involving the surfaces of insoluble particles serving as ice nuclei (IN) [e.g., *Vali*, 1985; *Cantrell and Heymsfield*, 2005]. The insoluble particles can either be bare (deposition nuclei) or immersed in larger, liquid particles (immersion nuclei). The terms bare and immersed refer to the state of mixing of the IN with other chemical components of the atmospheric aerosol. As bare particles age in the atmosphere, they acquire liquid surface coatings by condensing soluble species and water vapor or by scavenging soluble particles, and are thereby transformed into immersion nuclei. This transformation may dampen the ice-forming ability of some IN types [e.g., *Möhler et al.*, 2008; *Cziczo et al.*, 2009a; *Koehler et al.*, 2010].

[4] The level of basic scientific understanding of heterogeneous nucleation of ice in the troposphere is judged to be very poor [*Cantrell and Heymsfield*, 2005; *Kärcher and Spichtinger*, 2009]. In situ measurements suggest that atmospheric IN are mostly composed of mineral dust, carbonaceous material including black carbon (BC), and metallic particles [e.g., *Chen et al.*, 1998; *DeMott et al.*, 2003]. The field measurements, however, could not provide causal links between ice formation and IN composition. Insoluble particles show considerable variability in terms of chemical composition, location, frequency of occurrence, and number concentration. Their concentration mostly is much higher than the observed IN concentrations [e.g., *Rogers et al.*, 1998; *Minikin et al.*, 2003]. It is still not clear which microphysical and chemical properties enable only a specific fraction of the insoluble particles to form ice in clouds.

[1]Deutsches Zentrum für Luft- und Raumfahrt, Institut für Physik der Atmosphäre, Oberpfaffenhofen, Germany.
[2]Institute of Atmospheric and Climate Science, ETH Zürich, Zurich, Switzerland.

0148-0227/11/2010JD015302

[5] Heterogeneous nucleation of ice at cirrus temperatures (T below the homogeneous freezing temperature of pure water droplets $T_{hom} \simeq 235$ K) was mainly studied in the laboratory, either focusing on ice formation due to BC (soot) particles [e.g., *DeMott et al.*, 1999; *Möhler et al.*, 2005; *DeMott et al.*, 2009; *Koehler et al.*, 2009] or mineral dust particles [e.g., *Zuberi et al.*, 2002; *Archuleta et al.*, 2005; *Möhler et al.*, 2006; *Field et al.*, 2006; *Welti et al.*, 2009; *Koehler et al.*, 2010]. These studies reveal that heterogeneous nucleation can occur at relative humidities below the critical values for homogeneous freezing (i.e., between 100% and ~150% over ice), depending on composition, mixing state, and size of the IN. Most of these studies, however, were performed for conditions that are not fully representative of the atmosphere. This mostly precludes the immediate use of laboratory data in model applications.

[6] Heterogeneous and homogeneous ice formation compete for the available water vapor in the presence of IN. This competition ultimately determines the number of ice particles [*DeMott et al.*, 1997]. Heterogeneous ice nucleation can lead to a significant reduction of the number of ice particles that would form via homogeneous freezing in the absence of IN in otherwise unchanged conditions. IN may also prevent homogeneous freezing from occurring, in which case the number of ice crystals either decreases or slightly increases [*Kärcher et al.*, 2006] relative to a case without IN. Exactly how the ice particle number concentrations change depends mainly on temperature, the cooling rate, as well as on the number concentration and ice formation ability of the IN [*Kärcher et al.*, 2006].

[7] The first global climate model studies that assessed effects of aerosol changes on cirrus considered either homogeneous or heterogeneous ice formation, neglecting their competition [*Kärcher and Lohmann*, 2002; *Lohmann and Kärcher*, 2002; *Kärcher and Lohmann*, 2003; *Lohmann et al.*, 2004]. The prerequisites required in these studies to simulate aerosol indirect effects on ice clouds in the European Centre/Hamburg (ECHAM) general circulation model (GCM) were the development of parameterization schemes for pure homogeneous and heterogeneous ice nucleation and the introduction of a two-moment (total cloud ice mass and ice particle number concentration) ice microphysics scheme. To study the potential of BC particles from aviation to alter cirrus microphysical properties, *Hendricks et al.* [2005] considered a simplified representation of the competition in ECHAM by assuming that heterogeneous nucleation inhibits homogeneous freezing completely when the IN number concentration exceeds a threshold [*Gierens*, 2003]; at lower IN levels, pure homogeneous nucleation was considered. Along the same lines, ECHAM was applied by *Abbatt et al.* [2006] to study the effect of crystalline ammonium sulfate as an IN and by *Cziczo et al.* [2009b] to investigate the effect of mineral dust particles doped with lead. These first global model studies hinted at the potential of heterogeneous ice nucleation to affect cirrus on the large scale (resolved by GCMs). Distinctive changes in global mean ice crystal number, ice water path, as well as cloud radiative forcing were simulated.

[8] Several parameterization schemes of aerosol-induced ice formation have been developed more recently, taking into account the competition between different ice formation processes [*Liu and Penner*, 2005; *Kärcher et al.*, 2006; *Barahona and Nenes*, 2009]. Contrary to the approaches of *Liu and Penner* [2005] and *Barahona and Nenes* [2009], the parameterization developed by *Kärcher et al.* [2006] also considers the effects of preexisting ice on cirrus formation (i.e., within the cloudy part of a global model's grid box). *Liu et al.* [2007] introduced a two-moment scheme for ice clouds and included the parameterization of *Liu and Penner* [2005] in the NCAR Community Atmospheric Model Version 3 (CAM3) GCM. This model was applied by *Liu et al.* [2009] to study the global effects of anthropogenic ice-forming aerosol on upper tropospheric clouds. The results suggest considerable changes in ice crystal number concentration, ice mass mixing ratio, cloud occurrence frequency, and water vapor in the upper troposphere and lowermost stratosphere (UTLS) region because of heterogeneous ice formation triggered by anthropogenic BC. These perturbations and their resulting radiative forcings should therefore be the subject of further research. The *Liu and Penner* [2005] parameterization was also applied as part of two-moment ice microphysical schemes to simulate the competition of heterogeneous nucleation on mineral dust and homogeneous freezing in two other recent GCM studies [*Gettelman et al.*, 2010; *Salzmann et al.*, 2010]. The results of *Gettelman et al.* [2010] reveal that mineral dust particles can play an important role in cirrus cloud formation globally.

[9] The previous global model studies mentioned above neglected the effect of preexisting cloud ice on new ice formation. The deposition of water vapor on preexisting cloud ice particles reduces the rate of increase of supersaturation (for a given cooling rate) and may therefore inhibit or modify further ice particle formation [*Kärcher et al.*, 2006]. It is therefore necessary to consider this effect in GCM studies of aerosol-induced cirrus formation.

[10] Cloud ice in GCMs is traditionally considered by merging all types of ice formed by different mechanisms into a single ice mode. Different microphysical properties of coexisting ice types cannot be simulated. Hence, the potentially large differences in optical properties, sedimentation rates, and, importantly, atmospheric residence times of ice formed by homogeneous freezing and ice formed on different types of IN are not resolved. Also the microphysical competition of different aerosol types for water vapor during formation and depositional growth of the individual types of ice is usually not properly represented. As the different ice types can be characterized by different mean sizes, ice removal rates due to (size-dependent) sedimentation might vary widely among the different ice types, pointing at the need to parameterize this loss process properly in a GCM framework. Therefore, it is desirable to develop microphysical ice cloud schemes for GCMs which consider different coexisting ice types. Such schemes would allow the simulation and assessment of differences in the microphysical and optical properties of multiple ice types, albeit at the cost of enhanced microphysical complexity in the GCM cloud scheme.

[11] In the present work, we go one step further than previous studies and split the single cloud ice mass and total ice particle number concentration into the contributions of different ice types. We will refer to these different ice types distinguished by the model as ice modes. Each ice mode originates from a specific ice formation mechanism (either ice formation in cirrus induced by specific aerosol types or stemming from other mechanisms, such as glaciation of water clouds and deep convective outflow). The

introduction of multiple ice modes allows us to carefully evaluate global changes in cirrus microphysical properties due to different types of IN in a number of sensitivity experiments and to analyze the role of IN in cirrus formation and evolution in unprecedented detail. We further consider preexisting ice within the nucleation parameterization [*Kärcher et al.*, 2006] and during large-scale depositional growth in the GCM cloud scheme.

[12] In particular, we study and estimate the effects of IN on ice particle number concentration, cloud ice water content, cloud occurrence frequency, cirrus formation pathways, and water vapor in the UTLS region. We also study IN-induced changes in the frequency of occurrence of ice from homogeneous freezing. We make a first attempt to assess the specific roles of mineral dust particles, and black carbon aerosols from surface sources and from jet aircraft emissions (excluding effects of aircraft contrails), in cirrus formation. We refer to *Burkhardt et al.* [2010] for a discussion of research issues related to the climatic effects of contrail-induced cirrus clouds.

[13] Section 2 provides descriptions of the base model as well as the modifications of the microphysical cloud scheme applied in this study. Different model experiments are characterized. Model results on the effects of different IN types on global cirrus properties are discussed in section 3, including a comparison with observations. Conclusions and recommendations for future research are given in section 4.

2. Model and Methodology

[14] In the global model study by *Hendricks et al.* [2005], the ECHAM4 GCM [*Roeckner et al.*, 1996] was applied, including a two-moment cloud microphysical scheme and a simplified representation of the competition between homogeneous and heterogeneous ice formation in cirrus (section 1). The details of this model setup which is used as a base model for further development in the present study are described in section 2.1. The parameterization scheme developed by *Kärcher et al.* [2006] explicitly considers the competition between multiple ice modes during the cirrus formation process, including preexisting cloud ice. We have implemented this scheme into the base model, and at the same time, we have extended the single mode cloud ice microphysics into a multiple mode approach, whereby each ice mode is still represented by two moments, i.e., ice mass mixing ratio, q_{ice}, and ice particle number concentration, N_{ice}. The details of these modifications are described in section 2.2. The conceptual design of the set of simulations performed with the modified model is discussed in section 2.3.

2.1. Base Model

[15] The base model adopted here is the ECHAM4 GCM as applied by *Hendricks et al.* [2005]. Standard prognostic variables of ECHAM4 are vorticity, divergence, temperature, surface pressure, water vapor mass mixing ratio and cloud (liquid or ice) water mass mixing ratios. The model includes physical parameterizations of radiation, cloud processes, precipitation, convection, diffusion, planetary boundary layer dynamics, land surface processes and gravity wave drag. As an extension of the ECHAM4 standard version, the version applied here includes an aerosol scheme and a two-moment cloud scheme.

[16] The aerosol scheme solves prognostic equations for the mass mixing ratios of the major aerosol species sulfate, organic and black carbon, mineral dust, and sea salt [*Feichter et al.*, 1996; *Lohmann et al.*, 1999, 2004]. Separate prognostic equations are included to track black carbon from aircraft [*Hendricks et al.*, 2004]. The cloud scheme includes prognostic equations for the cloud liquid water content and the cloud droplet number concentration, as well as the ice water content and the ice particle number concentration in stratiform clouds [*Lohmann and Roeckner*, 1996; *Lohmann et al.*, 1999; *Lohmann*, 2002; *Lohmann and Kärcher*, 2002]. We apply a version of the cloud scheme updated according to *Lohmann et al.* [2003, 2004]. The model treats rain and snow diagnostically, taking into account flux modifications due to reevaporation or interactions with cloud water and ice. Subgrid-scale (fractional) cloud cover is diagnosed from the grid mean relative humidity [*Sundqvist et al.*, 1989] in regions that are subsaturated. To enable the simulation of cirrus cloud formation by homogeneous freezing requiring high supersaturations with respect to ice, the original saturation adjustment scheme was replaced by a diffusional growth scheme that permits ice supersaturation on the resolved scale [*Lohmann and Kärcher*, 2002], at the cost of abandoning the fractional cloud coverage in ice-supersaturated areas. The *Sundqvist et al.* [1989] scheme assumes that the cloud fraction increases from zero to unity for grid mean relative humidity values increasing from a critical threshold value ($\mathrm{RH}_0 < 1$) to saturation ($\mathrm{RH} = 1$). This implies that cirrus cloud coverage is zero as long as no nucleation takes place and one otherwise. The introduction of ice supersaturation and its consistent treatment together with fractional cirrus coverage and ice microphysics requires the use of a prognostic cloud fraction variable [*Kärcher and Burkhardt*, 2008], among other major modifications, which is beyond the scope of our study. Together with statistical noise issues explained later, this is the main reason why we focus on IN-induced changes in cirrus microphysical properties at this point and refrain from estimating radiative forcings associated with these potential cloud changes.

2.2. Microphysics of Multiple Ice Modes

2.2.1. General Concept

[17] The multiple ice mode approach applied here is particularly designed for simulations of IN effects on cirrus. A schematic overview of the different ice modes and the cloud physical processes considered is shown in Figure 1. Three ice modes are considered to represent cloud ice formed in the cold cloud regime ($T < T_{\mathrm{hom}}$). These modes comprise individual ice types formed by heterogeneous nucleation on mineral dust and on BC particles, and by homogeneous freezing of liquid aerosol. They are referred to as the het-du, het-bc, and hom modes, respectively. A fourth ice mode, the misc mode, is included to represent ice particles from other sources, such as spontaneous freezing of supercooled cloud droplets, detrainment of cloud ice from deep convective clouds, or IN-induced deposition-condensation nucleation at warmer temperatures ($T_{\mathrm{hom}} \leq T < 0°\mathrm{C}$).

[18] For each additional mode i, two prognostic equations are included to represent the respective number concentrations, $N_{\mathrm{ice},i}$, and mass mixing ratios, $q_{\mathrm{ice},i}$. Liquid cloud water is still considered by a single mode with prognostic equations for the total liquid water content and the total

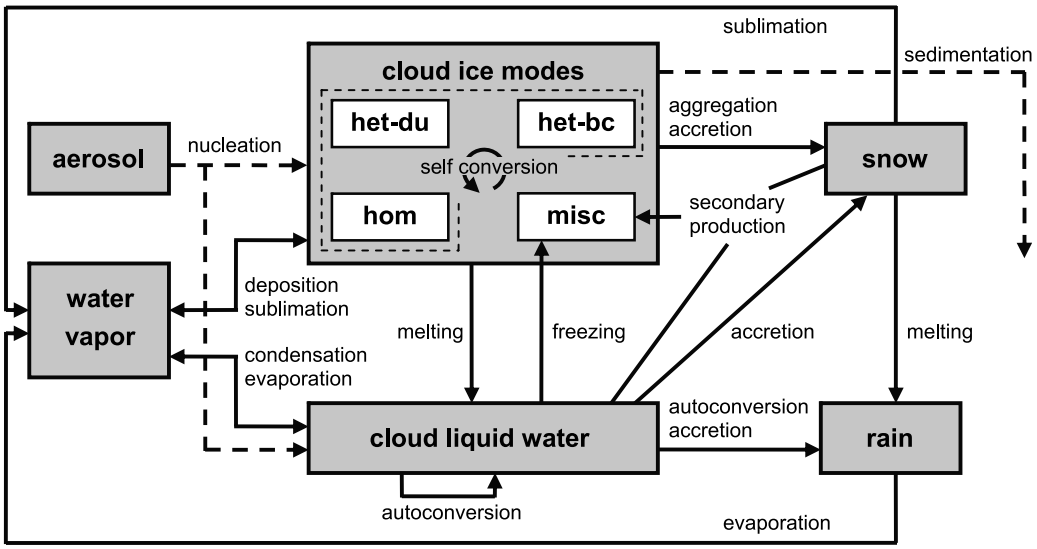

Figure 1. Schematic of the physical processes considered in the multiple–ice mode cloud scheme. Cloud ice is represented by four individual ice modes containing ice from heterogeneous nucleation on mineral dust (het-du) and black carbon (het-bc), ice from homogeneous freezing of liquid aerosols (hom), and ice from other sources (misc). Here accretion refers to the growth of snow crystals or rain droplets due to collection of cloud particles. Aggregation, self-conversion, and autoconversion refer to collision interactions of cloud ice particles or cloud droplets among themselves.

droplet number concentration. Cloud ice and liquid water can be transformed into precipitating hydrometeors (snow and rain) via particle-particle interactions and particle growth due to the uptake of water from the gas phase. Snow or rain is assumed to precipitate within one time step of the model (30 min) or is subject to sublimation or evaporation below a cloudy grid box, depending on the vertical distribution of relative humidity. In the case of cloud ice, a critical volume equivalent diameter of 200 μm [*Levkov et al.*, 1992] is used to separate snow from (pristine) cloud ice.

[19] In the microphysical cloud scheme of the base model, cloud ice is influenced by a number of processes: (1) formation via homogeneous freezing of liquid aerosols or heterogeneous ice nucleation, spontaneous freezing of supercooled cloud droplets, and secondary production of cloud ice due to collisions of cloud droplets with snow (Hallett-Mossop mechanism), (2) mass exchange with the gas phase via deposition of water vapor or sublimation of cloud ice, (3) aggregation of cloud ice particles and growth of snow crystals by accretion of cloud ice leading to the partial transformation of cloud ice particles to snow, (4) spatial redistribution of cloud ice due to advective, convective, and diffusive transport, as well as sedimentation, and (5) transformation into liquid cloud water via melting.

[20] The modifications necessary to represent these processes in the multiple ice mode approach are described below. If not otherwise mentioned, microphysical processes which apply to the individual ice modes, are represented as in the base model. We summarize these modifications to the original scheme in Table 1.

2.2.2. Cloud Ice Particle Formation

[21] In the cold cloud regime ($T < T_{\mathrm{hom}}$), aerosol-induced homogeneous and heterogeneous ice formation is calculated by the parameterization of *Kärcher et al.* [2006]. The parameterization uses an estimate of the subgrid-scale updraft speed (see below) and the relative humidity over ice (RHI) from the host model as input parameters and checks whether ice nucleation conditions can be reached within a time step of the host model. If so, the parameterization calculates the resulting modifications of the ice particle populations in the individual ice modes, occurring within that time step. The effect of preexisting ice is to slow the rate of increase in RHI due to depositional growth. This is expressed in terms of a reduced updraft speed. Using this reduced updraft speed, the nucleation of new crystals is either suppressed or their number can be reduced.

[22] For the present simulations, the parameterization was adjusted to the particular modal concept followed here considering the competition of two ice modes formed by heterogeneous nucleation on mineral dust and BC particles, ice formed because of homogeneous freezing of liquid aerosol, and ice from other sources. The parameterization requires a set of input parameters. In particular, the particle number concentrations, size distributions, and ice nucleation properties (see below) of the individual aerosol types forming the different ice modes, as well as the number concentration and mean size of preexisting ice particles in each ice mode need to be specified. Owing to the lack of appropriate atmospheric data (section 1), we assume monodisperse IN populations, using characteristic mean sizes and sharp $\mathrm{RHI_{crit}}$ values, the latter describing the onset relative humidities over ice of heterogeneous ice nucleation. Results are sensitive to $\mathrm{RHI_{crit}}$ (but less to the IN size in the parameterization as long as the sizes are not chosen unrealistically small [*Kärcher et al.*, 2006]). Therefore, we will vary the $\mathrm{RHI_{crit}}$ values in sensitivity experiments (section 2.3). The parameterization determines the fraction of the IN population that nucleates ice. This fraction increases to unity for sufficiently large updraft speeds. Additional input parameters of the parameterization are the ambient pressure,

Table 1. Summary of Modifications to the Original Cloud Scheme

Feature	Reference Scheme	Modified Scheme
Ice formation at cirrus temperatures ($T < T_{hom}$)	Either homogeneous freezing of liquid aerosols or heterogeneous ice nucleation [*Kärcher and Lohmann*, 2002, 2003], no competition between ice modes during ice formation	Competition of heterogeneous ice nucleation on mineral dust and black carbon, homogeneous freezing of liquid aerosols, and preexisting cloud ice [*Kärcher et al.*, 2006]
Ice modes	Single ice mode	Four separate modes representing ice from heterogeneous nucleation on mineral dust (het-du), heterogeneous nucleation on black carbon (het-bc), homogeneous freezing of liquid aerosol (hom), and other mechanisms (misc)[a]
Prognostic equations	5 (for q_v, q_{liq}, N_{liq}, q_{ice}, N_{ice})[b]	11 (for q_v, q_{liq}, N_{liq}, $q_{ice,i}$, $N_{ice,i}$, $i \in \{1,\ldots,4\}$)[c]
Ice depositional growth and sublimation	Uniform growth and sublimation of ice mass	Competitive growth and sublimation of ice mass in different modes
Particle-particle interactions	Parameterized aggregation and accretion applied to single ice mode[d]	Parameterized aggregation applied to the total ice population, parameterized accretion applied to the individual modes[d,e]
Ice transport and sedimentation	Applied to total ice	Applied to individual modes

[a]The misc mode is formed by (1) heterogeneous deposition-condensation nucleation at temperatures $T_{hom} \le T < 0°C$, (2) freezing of supercooled cloud droplets in stratiform clouds, (3) secondary production of ice particles due to collisions of cloud droplets with snow, and (4) detrainment of cloud ice from deep convective clouds.

[b]Here q_v, q_{liq}, q_{ice}, N_{liq}, and N_{ice} denote the water vapor mixing ratio, the liquid and ice water mixing ratios, and the cloud droplet and ice crystal number concentrations.

[c]Here $q_{ice,i}$ and $N_{ice,i}$ denote the ice water mixing ratio and crystal number concentration of ice mode i.

[d]Here accretion refers to the collection of cloud ice particles by snow crystals, while aggregation refers to collision interactions of cloud ice particles among themselves.

[e]For a description of the representation of collision interactions of particles from different modes, see section 2.2.4.

temperature, relative humidity, the large-scale model time step, and a mesoscale vertical velocity taken from the model's turbulent kinetic energy budget [*Lohmann and Kärcher*, 2002; *Lohmann et al.*, 2004]. Typical values of the mesoscale vertical velocity generated by the model are in the range of 1–100 cm s^{-1} under cirrus formation conditions. Using a single value of the updraft speed in combination with the grid mean RH instead of applying probability distributions is a simplification. The updraft speed, however, is determined by adding a subgrid-scale component of the updraft speed on the basis of the turbulent kinetic energy to the large-scale vertical velocity such that realistic cirrus properties are obtained. The parameterization returns the modified ice particle number concentration and mean size in each ice mode, which are reformulated as nucleation source terms for use in the N_{ice} and q_{ice} tracer equations in the climate model. The nucleation source terms for the ice particle number concentrations $N_{ice,i}$ of the individual modes i are

$$\left.\frac{\partial N_{ice,i}}{\partial t}\right|_{nucl} = \frac{N_{ice,i}^{nucl} - N_{ice,i}^{old}}{\Delta t}, \quad (1)$$

where $N_{ice,i}^{nucl}$ are the modified ice particle number concentrations returned from the parameterization, $N_{ice,i}^{old}$ are the number concentrations of the preexisting ice particles used as input for the parameterization, and Δt is the model time step. $N_{ice,i}^{nucl}$ and $N_{ice,i}^{old}$ are identical if nucleation of new ice particles does not occur. The representation of the nucleation effects on $q_{ice,i}$ in the model are discussed in section 2.2.3. Cloud ice generated by heterogeneous nucleation on mineral dust and BC particles is assigned to the het-du and het-bc modes, respectively. Ice formed via homogeneous freezing of liquid aerosols is assigned to the hom mode.

[23] The RHI_{crit} values are chosen to match experimental data (section 2.3). The preexisting mean ice particle sizes of each ice mode are calculated from the respective number concentration and ice water content assuming monodisperse size distributions and spherical ice particles. The aerosol properties assumed for driving the ice nucleation parameterization are summarized in Table 2. The number concentration of hygroscopic aerosol particles available for homogeneous freezing is derived from the mass concentrations of liquid solution aerosol compounds according to *Lohmann et al.* [2004] by assuming typical background aerosol size distributions. The minimum number of aerosol particles assumed to always be present is 10 particles cm^{-3} in accordance with observations taken at midlatitudes and in the tropics [*Minikin et al.*, 2003]. The sizes of liquid particles are identified with the median sizes of the assumed size distributions. Similarly, the number concentration of mineral dust particles is derived from the mineral dust mass concentration. Only the dust mass present in the submicron size range [*Lohmann et al.*, 2004] is considered since the number concentration of coarse mode dust particles is probably negligible in the upper troposphere. Particle number concentrations are derived assuming representative size distributions of large Aitken and accumulation mode dust recommended by *Hess et al.* [1998] (Table 2). Number concentrations of BC particles from surface sources are calculated from the simulated mass concentrations assuming typical number-to-mass ratios [*Hendricks et al.*, 2004] (Table 2). To investigate the maximum potential of BC from aircraft to perturb cirrus clouds (sections 2.3 and 3), we use the maximum estimate approach defined by *Hendricks et al.* [2004] to calculate number concentrations of BC from aircraft. In this approach, BC number-to-mass ratios typical for fresh aircraft exhaust are considered and, reductions in number-to-mass ratio due to aging processes are neglected.

[24] We have confidence in the parameterization of the homogeneous freezing process; more uncertainties exist for specifying heterogeneous ice nucleation. A first-order problem associated with the latter is the knowledge of the fraction of the total aerosol (dust or BC) population that is actually able to form ice in the atmosphere (ice active fractions, f). Ice active fractions vary considerably. Labo-

Table 2. Summary of Aerosol Properties

Aerosol Type	Size Distribution[a]	Ice Nucleation Properties[b]
Mineral dust	Mode 1: d_1 = 140 nm, σ_1 = 1.95; mode 2: d_2 = 780 nm, σ_2 = 2.00; N_1/N_2 = 8.84 [*Hess et al.*, 1998]	f = 1%, RHI_{crit} = 130%, d_{frz} = 205 nm[c]
Black carbon from surface sources	Primary spheres: d = 23.6 nm, σ = 2.0 [*Hess et al.*, 1998], particles are assumed to be aggregates formed of 10 primary particles [*Hendricks et al.*, 2004]	f = 0.25%, RHI_{crit} = 140% or 120%, d_{frz} = 67 nm[c,d]
Black carbon from aircraft	Prognostic equations solved for particle number concentrations using maximum estimate approach by *Hendricks et al.* [2004]	f = 10%, RHI_{crit} = 120%, d_{frz} = 33 nm[c,e]
Liquid solution particles	Size distributions according to *Lohmann et al.* [2004]	homogeneous freezing, d_{frz} according to median diameters

[a]Size distribution assumed to calculate particle number concentrations. Lognormal number size distribution parameters: median diameter d, geometric standard deviation σ, and total number concentration N of particles within mode.

[b]Here f denotes the assumed ice active number fraction, and d_{frz} denotes the particle size of the monodisperse particle population assumed for ice nucleation calculations (section 2.2.2). For multimodal distributions, d_{frz} is identified with the particle number weighted average of the mode median diameters.

[c]The particle size assumed here only affects the ice nucleation rate in the heterogeneous nucleation parameterization. The relative humidity threshold RHI_{crit} is not affected. The results of the parameterization are sensitive to RHI_{crit} (but less to the ice nuclei size as long as the sizes are not chosen unrealistically small).

[d]Volume equivalent diameter of aggregates, assuming specific densities of 1.0 g cm^{-3} for aggregates and 2.3 g cm^{-3} for primary spheres.

[e]Median diameter of aircraft-induced black carbon size distribution [*Döpelheuer*, 2002].

ratory measurements demonstrate that only very small fractions (typically $f < 0.1\%$ −1%) of the available black carbon particles constitute the ice active fraction and can therefore act as IN [e.g., *Koehler et al.*, 2009]. Mineral dust particles in the laboratory showed considerably higher ice active fractions ranging from less than 0.1% at low supersaturation to values of several 10% close to the homogeneous freezing threshold [e.g., *Field et al.*, 2006; *Möhler et al.*, 2006; *Welti et al.*, 2009]. The ice active fractions of dust particles in the atmosphere, however, could be much smaller since the particles might be coated with liquid solutions which can drastically reduce the fraction of particles serving as deposition nuclei at supersaturations well below the homogeneous freezing threshold [e.g., *Möhler et al.*, 2008; *Cziczo et al.*, 2009a]. It is not clear which factors actually control f for a given type of atmospheric IN. Source characteristics and atmospheric aging processes play a role, likely affecting both f and RHI_{crit} at the same time.

[25] Small f values are also consistent with in situ data taken at northern midlatitudes [*Minikin et al.*, 2003], pointing at total number concentrations of refractory (presumably insoluble) particles of 10–100 cm^{-3}. These concentrations are much higher than background IN concentrations (~0.01 cm^{-3}) estimated in the same area [*Haag et al.*, 2003], allowing us to indirectly infer an upper limit ice active fraction $f \simeq 0.1\%$ of refractory aerosols from these data. Hence, these hints are available on how to constrain f, but a clear picture has not yet emerged.

[26] Therefore, we can only very roughly include ice active fractions in the simulations at this point. We estimate the actual IN number concentrations, N_{IN}, from the total number concentrations, N, via

$$N_{IN}(BC) = f_{BC} N(BC)$$

$$N_{IN}(DU) = f_{DU} N(DU). \quad (2)$$

N(BC) and N(DU) are the total number concentrations of BC and dust particles, respectively, and f_{BC} and f_{DU} are their ice active fractions ($0 \le f \le 1$), which are assumed to be constant for each individual IN type. N_{IN}(DU) and N_{IN}(BC), together with the corresponding RHI_{crit} values, are used as input for the ice nucleation parameterization. As mentioned above, only a fraction of the total N_{IN} might nucleate ice, depending on the updraft speed. This fraction increases to unity for sufficiently large updraft speeds. Setting $f = 1$ would dramatically overestimate the effect of dust and BC particles on cirrus properties. While we capture this effect in our simulations by specifying values $f \ll 1$ (section 2.3), a better understanding of factors controlling ice active fractions is needed in order to make progress in this field. This is necessary, because even advanced global aerosol models capable of predicting N provide no clues on how to calculate f. Although we believe that it is sufficiently detailed for current GCM applications, the assumption of fixed ice active fractions in combination with sharp RHI_{crit} values in our model is a simplification since measured freezing spectra show ice active fractions increasing continuously with relative humidity.

[27] Heterogeneous ice nucleation is also allowed to occur in the mixed-phase cloud regime ($T_{hom} \le T < 0°C$), where ice and supercooled liquid water may coexist. We consider freezing of cloud droplets initiated by immersion and contact freezing in stratiform clouds as described by *Levkov et al.* [1992] and *Lohmann* [2002]. The number of new ice crystals formed in this temperature regime via heterogeneous deposition-condensation nucleation (no cloud droplets involved) is obtained from the parameterization developed by *Meyers et al.* [1992]. Comparisons of the results of this parameterization with measurements reveal that it provides IN number concentrations at the large end of the observed values [*DeMott et al.*, 2010]. Ice particles generated via these mechanisms are assigned to the misc mode. Further mechanisms leading to cloud ice assigned to the misc mode

include (1) homogeneous freezing of supercooled cloud droplets in stratiform clouds at temperatures $T < T_{\mathrm{hom}}$, (2) secondary production of ice particles due to collisions of cloud droplets with snow [*Levkov et al.*, 1992; *Lohmann*, 2002], and (3) detrainment of cloud ice from deep convective clouds. To realize mechanism 3, ice particle numbers are derived from the amount of detrained cloud ice assuming spherical particles with a mean diameter of 60 μm. This value was derived by transforming ice particle size distributions measured in convective outflow [*McFarquhar and Heymsfield*, 1997] into a monodisperse population.

2.2.3. Depositional Growth and Sublimation

[28] The inclusion of the ice nucleation parameterization by *Kärcher et al.* [2006] in combination with the multiple ice mode approach necessitates additional modifications in the treatment of large-scale water deposition. Depositional growth and sublimation of cloud ice is simulated as done by *Lohmann and Kärcher* [2002]. Diffusional growth rates are calculated for each mode depending on the mean ice particle size and number concentration. When new cloud ice forms via nucleation at $T < T_{\mathrm{hom}}$, the different ice modes form successively in the parameterization in the order of increasing nucleation relative humidities, $\mathrm{RHI}_{\mathrm{crit}}$. Therefore, large-scale growth rates of the different ice modes in the GCM cloud module have to be estimated over different fractions of the model time step. The gain in ice mass during the nucleation event could be directly taken from the parameterization. This, however, would imply the use of a depositional growth formulation (suited for the freshly nucleated ice particles) different from the standard formulation applied in the GCM. The depositional growth of ice formed during a nucleation event would also be calculated by considering the relative humidities in the mesoscale updrafts, which can be considerably higher than the large-scale average values. This would imply inconsistencies between the depositional growth during aerosol-induced cirrus formation described by the parameterization and the growth of aged cirrus ice or ice from other sources described by the GCM's standard deposition formulation. Therefore, we generally calculate the depositional growth of the particles in the individual ice modes according to the standard formulations of the GCM, but redistribute the total deposited mass according to the gain in ice mass in each mode as calculated by the nucleation parameterization when aerosol-induced ice nucleation occurs under cirrus conditions. This is achieved as follows. The gain in ice mass mixing ratio $\Delta q_{\mathrm{ice},i}^{\mathrm{nucl}}$ (mass of ice per mass of air) in each ice mode i, as determined by the ice nucleation parameterization for the large-scale model time step including the nucleation event, can be calculated as

$$\Delta q_{\mathrm{ice},i}^{\mathrm{nucl}} = \frac{\rho_{\mathrm{ice}}}{\rho_{air}} \frac{\pi}{6} \left[N_{\mathrm{ice},i}^{\mathrm{nucl}} \left(D_{\mathrm{ice},i}^{\mathrm{nucl}} \right)^3 - N_{\mathrm{ice},i}^{\mathrm{old}} \left(D_{\mathrm{ice},i}^{\mathrm{old}} \right)^3 \right], \qquad (3)$$

where ρ_{ice} and ρ_{air} are the densities of ice and air, respectively, $N_{\mathrm{ice},i}^{\mathrm{nucl}}$ and $D_{\mathrm{ice},i}^{\mathrm{nucl}}$ are the ice particle number concentration (ice particle number per volume of air) and diameter of mode i as returned from the parameterization, and $N_{\mathrm{ice},i}^{\mathrm{old}}$ and $D_{\mathrm{ice},i}^{\mathrm{old}}$ are the particle number concentration and diameter of mode i before nucleation (used as input for the parameterization). If ice nucleation occurs, the temporal change in ice mass mixing ratio due to water vapor deposition in each individual mode i is calculated by redistributing the depositing ice mass as follows:

$$\left. \frac{\partial q_{\mathrm{ice},i}}{\partial t} \right|_{\mathrm{dep}} = \frac{1}{\Delta t} \frac{\Delta q_{\mathrm{ice},i}^{\mathrm{nucl}}}{\sum_j \Delta q_{\mathrm{ice},j}^{\mathrm{nucl}}} \sum_j \Delta q_{\mathrm{ice},j}^{\mathrm{dep}}, \qquad (4)$$

where $\Delta q_{\mathrm{ice},j}^{\mathrm{dep}}$ is the gain in ice mass mixing ratio of mode j due to water vapor deposition within the time step Δt, calculated according to the GCM deposition formulation [*Lohmann and Kärcher*, 2002, equation (2)] by considering the updated ice particle number concentration $N_{\mathrm{ice},j}^{\mathrm{nucl}}$.

[29] Because of the limited number of IN, heterogeneous ice nucleation results in low ice particle number concentrations. The few particles formed can grow to large sizes, particularly when preexisting ice, or ice from homogeneous freezing potentially formed shortly after heterogeneous nucleation, is absent. Such large particles will settle quickly. To avoid numerical instabilities due to sedimentation of cloud ice through multiple model layers, ice particles are transformed into snow, when their volume equivalent diameter increases beyond 200 μm (section 2.2.1).

2.2.4. Particle-Particle Interactions

[30] Model-based analyses of in situ measurements in deep frontal clouds and stratiform cirrus demonstrate that the growth of small ice crystals in such clouds is dominated by water vapor deposition while the growth of large particles, with comparatively lower number concentrations and larger sizes of several 100 μm, is dominated by aggregation [*Kajikawa and Heymsfield*, 1989; *Field*, 2000; *Field and Heymsfield*, 2003]. This finding has recently been confirmed and interpreted by cloud-resolving simulations [*Sölch and Kärcher*, 2011]. Aggregates dominate the large end of the ice particle size distribution (maximum ice particle dimensions >1–2 mm) and their number concentration (<0.001 cm^{-3}) is many orders of magnitude lower than that of pristine crystals.

[31] As mentioned above, large ice particles are assigned to the precipitation (snow) mode in our model (section 2.2.1). The further growth of snow due to aggregation is represented by the accretion process, i.e., the collision and sticking with smaller cloud ice particles. As in the original single mode scheme, we simulate this process according to the accretion approach by *Levkov et al.* [1992] applied to each individual ice mode.

[32] The conversion of cloud ice to snow due to self-aggregation of cloud ice particles is also considered. As discussed above, this process is probably of secondary importance in the model and is therefore treated in a simplified way: As in the original model, the loss of total cloud ice mass (q_{ice}) due to this process is estimated according to the *Levkov et al.* [1992] aggregation formulation. This approach takes into account the dispersion of the cloud ice crystal fall velocity spectrum assuming a typical crystal size distribution. Such a pseudospectral representation is necessary here because of the simplifying assumption of monodisperse ice particle size distributions which does not allow for aggregation calculations based on modeled size spectra. In the case of coexistence of different cloud ice modes, simplifying assumptions have been made to represent the effect of snow formation by aggregation on the individual ice modes: The loss of $q_{\mathrm{ice},i}$ within the modes i is estimated

by partitioning the total loss in proportion to their contributions $q_{\mathrm{ice},i}$ to the total q_{ice}. Following the work of *Levkov et al.* [1992], it is further assumed that the ice crystal number concentrations $N_{\mathrm{ice},i}$ are depleted in proportion to $q_{\mathrm{ice},i}$. With these simplifying assumptions, the information about the contributions of ice from the different sources is conserved.

[33] Self-conversion of cloud ice due to aggregation (aggregates formed are still in the size range of cloud ice particles and are not transferred to snow) is treated analogously, with the difference that this process only affects the crystal number concentrations. The total loss of N_{ice} is calculated according to the work by *Levkov et al.* [1992]. The loss of $N_{\mathrm{ice},i}$ within the modes i is then estimated by partitioning the total loss in proportion to their contributions $N_{\mathrm{ice},i}$ to the total N_{ice}.

[34] We are aware that the simplified representation of aggregation due to collisions of cloud ice particles can be a source of uncertainties. Although the effect of these uncertainties is probably limited, a more detailed treatment of aggregation in two-moment ice microphysical schemes should be the subject of future research.

2.2.5. Transport and Sedimentation of Cloud Ice

[35] Each ice mode is subject to transport due to advection, convection, and turbulent diffusion, resulting in spatial redistribution of the individual ice mass and number concentration [*Lohmann and Roeckner*, 1996; *Lohmann*, 2002]. The treatment of the ice particle number concentration in the outflow of convective clouds has been described in section 2.2.2.

[36] In the original single-mode scheme, the vertical redistribution of cloud ice due to sedimentation is calculated by applying an empirical formulation for the terminal fall speed of ice particles, v_t, dependent on the in-cloud ice water content (IWC) in units of kg ice/kg air [*Heymsfield*, 1977]:

$$v_t = \alpha(\rho \mathrm{IWC})^{\beta}, \tag{5}$$

where ρ denotes the air density at cloud altitude in units of kg air/m^3 air. The empirical constants α and β are $\alpha = 1.65$ and $\beta = 0.16$, yielding v_t in units of m/s. The sole dependence of v_t on IWC does not allow IN effects on cirrus to be studied in the microphysical part of the model, and does not make use of the additional information provided by N_{ice}.

[37] In the multiple mode scheme, sedimentation rates are calculated for each ice mode i taking into account an empirical formulation of the size-dependent terminal fall speeds v_t^i (m/s) [*Heymsfield et al.*, 2007]:

$$v_t^i = a\left(\overline{D}_{\mathrm{ice}}^i\right)^b \left(\frac{\rho_0}{\rho}\right)^{\kappa}, \tag{6}$$

where $\overline{D}_{\mathrm{ice}}^i \propto (\mathrm{IWC}^i/N_{\mathrm{ice}}^i)^{1/3}$ denotes the mean spherical ice particle diameter (m) within ice mode i, and ρ and ρ_0 are the air densities at cloud altitude and at the ground, respectively. The empirical constants a, b, and κ are chosen as $a = 700$ m/s, $b = 1$, and $\kappa = 1/3$ [*Murakami*, 1990].

2.2.6. Melting

[38] If temperatures increase above the melting point (0°C), cloud ice is transformed into cloud liquid water. The cloud liquid water content as well as the droplet number concentration are increased by the total ice water content and ice particle number concentration of melting cloud ice modes.

2.3. Description of the Simulations

[39] All model runs analyzed in the present study were performed for a 10 year time period following a 15 month model spin-up. The model is run at T30 spectral horizontal resolution, which corresponds to a horizontal grid size of about 3.8° × 3.8°. The vertical grid has 19 layers, ranging from the surface up to 10 hPa. For reasons of comparability, the emission data and other boundary conditions, such as sea surface temperatures and sea ice extent, are chosen as in the *Hendricks et al.* [2004, 2005] studies.

[40] The set of simulations performed to study the global effects of IN on cirrus with the multiple ice mode scheme is summarized in Table 3. A reference simulation (REF) with the original single ice mode scheme was performed to assess the effects of the modifications to the cloud scheme, such as the individual representation of specific ice types or the consideration of preexisting ice in the nucleation parameterization. In order to investigate the role of dust- and BC-derived (externally mixed) IN, we carried out a number of different simulations focusing on specific IN types. Also, the relative humidity thresholds for the onset of heterogeneous ice nucleation, $\mathrm{RHI}_{\mathrm{crit}}$, were varied. Heterogeneous ice nucleation under cirrus conditions is entirely neglected in the simulations REF and HOM, so that cirrus forms only via homogeneous freezing. While simulation REF employs the homogeneous freezing parameterization described by *Kärcher and Lohmann* [2002], simulation HOM is performed with the same model setup as the sensitivity experiments on IN effects described above, with the difference that the IN number concentration is set to zero in the call of the *Kärcher et al.* [2006] parameterization. The principle advantage of the *Kärcher et al.* [2006] parameterization over the *Kärcher and Lohmann* [2002] approach in such homogeneous freezing simulations is the consideration of preexisting ice.

[41] Laboratory measurements of heterogeneous ice formation under cirrus conditions, employing a number of dust particle types or, more commonly, surrogates of dust particles, show a large variety of ice nucleation characteristics, even within a single sample. Measured $\mathrm{RHI}_{\mathrm{crit}}$ values for the onset of ice nucleation in a significant fraction of the aerosol samples range from ~110% up to values near the homogeneous freezing threshold, ~150% [e.g., *Zuberi et al.*, 2002; *Archuleta et al.*, 2005; *Möhler et al.*, 2006; *Field et al.*, 2006; *Welti et al.*, 2009; *Koehler et al.*, 2010]. These threshold values seem to depend strongly on the dust particle size and composition. In our model, dust is represented by a single generalized species, rather than being split into different mineral compositions. However, different mineral types may exhibit different ice nucleation behavior. To simulate the overall dust effect on cirrus, we therefore choose a representative value of $\mathrm{RHI}_{\mathrm{crit}} = 130\%$ for dust IN, which lies about midway in the range of the laboratory measurements. Mineral dust particles are usually thought to be efficient IN. We refrain from assigning lower $\mathrm{RHI}_{\mathrm{crit}}$ values to mineral dust, as surface coatings developing during atmospheric processing possibly dampen the ice nucleation ability (sections 1 and 2.2.2). Dust particles emitted at the Earth's surface likely undergo such processing, poten-

Table 3. Summary of Model Runs

Simulation	Ice Nuclei (RHI_{crit})[a]	Multimodal
REF	No (homogeneous freezing only)	No
HOM	No (homogeneous freezing only)	Yes
HETDB	DU (130%), BC_{surf} (140%), hom[b]	Yes
HETBD	BC_{surf} (120%), DU(130%), hom[b]	Yes
HETD	DU (130%), hom[b]	Yes
HETA	BC_{surf} (120%), BC_{airc} (120%), DU (130%), hom[b]	Yes

[a]All details specified here refer to heterogeneous ice formation at temperatures $T < T_{hom}$. DU, BC_{surf}, and BC_{airc} denote mineral dust, black carbon from surface sources, and black carbon from aircraft, respectively.

[b]Heterogeneous ice nucleation competes with homogeneous freezing of liquid aerosols.

tially turning fresh, bare dust deposition nuclei into immersion nuclei. Hence, only a small uncoated fraction might reach the UTLS and affect cirrus formation via deposition freezing [*Wiacek et al.*, 2010].

[42] Similar arguments hold for BC or soot particles. A very wide range of ice nucleation characteristics, depending on the BC source, hygroscopic properties, and other factors, has been observed in the laboratory [e.g., *DeMott et al.*, 1999; *Möhler et al.*, 2005; *DeMott et al.*, 2009; *Koehler et al.*, 2009]. Hydrophilic BC particles coated by liquid supercooled solutions show values of RHI_{crit} that differ from those measured with uncoated (presumably less hydrophilic) BC particles, but the reasons are unclear. The state of knowledge on the ice-nucleating properties of BC particles at cirrus temperatures has been summarized by *Kärcher et al.* [2007]. According to their assessment, BC and BC-containing particles induce ice formation at RHI_{crit} = 105% −170%, but a systematic behavior is not obvious and the causes of the wide range of measured RHI_{crit} values are not understood. Therefore, as for mineral dust, a constant RHI_{crit} value is assumed in the model for BC. According to the measured range, the simulation HETDB (Table 3) was performed assuming a representative value of RHI_{crit} = 140%. Hence, heterogeneous nucleation on mineral dust (RHI_{crit} = 130%) occurs before and may even prevent ice formation on BC.

[43] BC shows a considerably large anthropogenic fraction. Possible anthropogenic climate perturbations caused by BC effects on cirrus could be of relevance in particular when a fraction of atmospheric BC would form ice efficiently. To assess such a scenario, an additional model experiment (HETBD) was performed where BC is assumed to form ice at a comparatively low critical supersaturation of RHI_{crit} = 120%. This might be an extreme assumption since it is not even clear from the observational data whether atmospheric BC particles are potent IN at all. Therefore, an additional sensitivity experiment (HETD) was carried out. In this simulation, BC particles do not act as IN at cirrus temperatures and, therefore, heterogeneous nucleation of cirrus ice particles only occurs on dust aerosol.

[44] Ice formation on BC particles from aircraft was neglected in the experiments described above. To study the potential role of this effect, a specific experiment (HETA) was performed, which is identical to HETBD with the exception that also ice formation on BC (soot) particles emitted by aircraft engines is considered, using RHI_{crit} = 120% as well. BC particles from aviation are included also in the other experiments, but do not form ice. To investigate the maximum potential of aircraft soot emissions to perturb cirrus, the rather low ice nucleation threshold, together with a high ice active fraction of f = 10% assumed for aircraft soot emissions and high particle number concentration estimates (section 2.2.2) serve to maximize the large-scale impact of aircraft, albeit against a background concentration of efficient IN particles from other sources (Table 3). The value of f = 10% was chosen according to the results of *Koehler et al.* [2009] who measured a comparatively high ice active fraction for soot particles from aircraft engines, although the corresponding critical relative humidities were distinctively higher in the measurements than the value of RHI_{crit} assumed here.

[45] To constrain f_{BC} for BC particles from surface sources and f_{DU} in equation (2), we rely on the results of in situ measurements. We assume f_{BC} = 0.25% and f_{DU} = 1% and thereby roughly match IN number concentrations and composition measured in the UTLS region over the Untied States during the SUCCESS field campaign [*Chen et al.*, 1998; *Rogers et al.*, 1998]. These airborne measurements reveal typical IN number concentrations of about 0.01 cm^{-3}, with similar contributions from carbonaceous and mineral particles. From these data, it is not clear which of these particles nucleated ice most efficiently. Specific information on aircraft-generated soot particles could not be derived from the SUCCESS data.

3. Results and Discussion

[46] In the following we will discuss general features of aerosols and ice clouds simulated with the modified model. Comparisons with observations are discussed in section 3.2. Changes in ice cloud properties due to the various assumptions on the ice formation ability of different aerosol types as investigated with the set of model experiments described in section 2.3 are discussed in section 3.3.

3.1. Aerosol and Ice Cloud Properties

3.1.1. Aerosol Number Concentration

[47] The simulated concentrations of aerosol particles that can potentially serve as IN are shown in Figure 2. Vertical distributions of zonally and annually averaged total (IN and non-IN) number concentrations of mineral dust and BC particles simulated in experiment HETDB are presented. Number concentrations of liquid solution aerosols used as input for the homogeneous freezing parameterization are also shown. The number concentrations were calculated as described in section 2.2.2. The mean UTLS (100–300 hPa) number concentrations of mineral dust particles are mostly in the range of 0.1–1 cm^{-3} (Figure 2a). Because of the larger land surface areas, mineral dust concentrations in the Northern Hemisphere are larger than in the Southern Hemisphere. The mean number concentration of BC particles from surface sources is presented in Figure 2b. The BC number concentrations typically exceed the dust concentrations by factors of 2–3. The sum of the concentrations of both particle types agrees well with our previous study [*Hendricks et al.*, 2005].

[48] Significant number concentrations of BC particles from aviation are simulated, particularly in the Northern

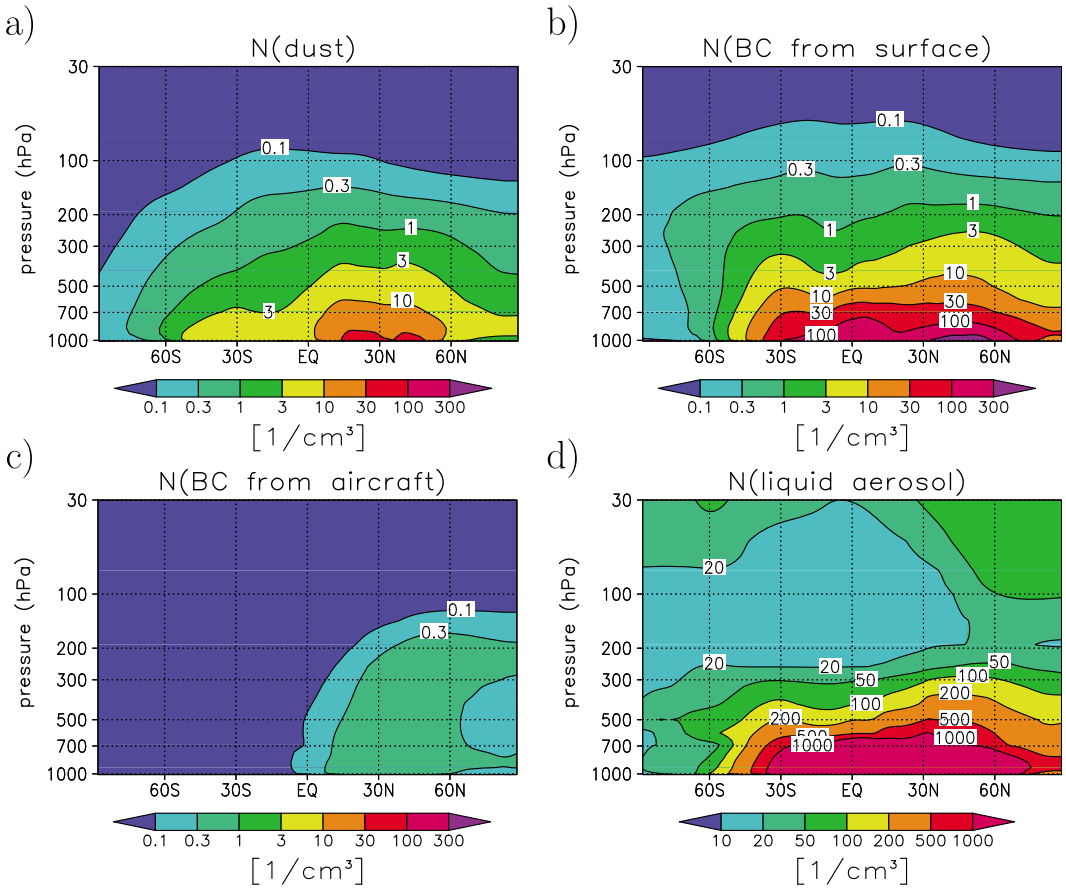

Figure 2. Vertical distributions of the zonally averaged annual mean particle number concentration of (a) mineral dust, (b) black carbon (BC) from surface sources, (c) BC from aircraft, and (d) liquid solution aerosols. Results are taken from simulation HETDB and represent 10 year averages. Note the different scale in Figure 2d.

Hemisphere (Figure 2c), in agreement with our earlier estimates [*Hendricks et al.*, 2004]. Mean number concentrations of up to 0.5 cm^{-3} occur in these areas. Thus, the contribution of BC from aviation to the total BC particle number concentration amounts up to 10%–20% in terms of zonal mean annual averages. *Liu et al.* [2009] simulated similar total number concentrations of BC particles from aircraft and from surface sources in their global model study. The annual mean upper tropospheric liquid aerosol particle number concentrations (Figure 2d) range between about 10 and several 100 cm^{-3}, with the largest values at northern midlatitudes. These number concentrations are in agreement with in situ measurements [e.g., *Petzold et al.*, 2002; *Minikin et al.*, 2003].

[49] The number concentrations of mineral dust and black carbon IN are calculated from the respective total concentrations according to equation (2) assuming IN fractions of 1% and 0.25% for mineral dust and BC from surface sources, respectively (section 2.3). This results in zonal mean annual average UTLS IN concentrations of 1–10 particles per liter of air for both particle types, broadly consistent with atmospheric data (section 2.3). For aircraft-generated BC, a comparatively large IN fraction of 10% is assumed leading to zonal mean annual average IN concentrations of up to 50 L^{-1} in the Northern Hemisphere UTLS region. These comparatively high IN concentrations apply only in simulation HETA. Ice formation on aircraft-produced BC particles is neglected in all other simulations (Table 3).

3.1.2. Ice Particle Number Concentration

[50] Figure 3 shows vertical distributions of zonal mean annual average number concentrations of cloud ice particles in the different modes from experiment HETDB, where the het-du mode forms before the het-bc mode in an ascending air mass. All-sky means are shown which were calculated by averaging over cloudy and cloud-free cases. Number concentrations of ice particles formed via heterogeneous nucleation in the ice modes het-du (Figure 3a) and het-bc (Figure 3b) show only small ice particle number concentrations, as expected, since the underlying IN populations show comparatively low number concentrations. The largest average ice particle concentrations of ~0.2 L^{-1} correspond to average in-cloud values of up to 1 L^{-1}.

[51] These in-cloud ice particle number concentrations are significantly smaller than the number concentrations of available IN, which is likely caused by efficient removal of large ice particles due to sedimentation and precipitation formation (section 2.2.3). Another possible reason is that not all available IN are activated at very low cooling rates [*Kärcher et al.*, 2006]. Under such conditions, only a

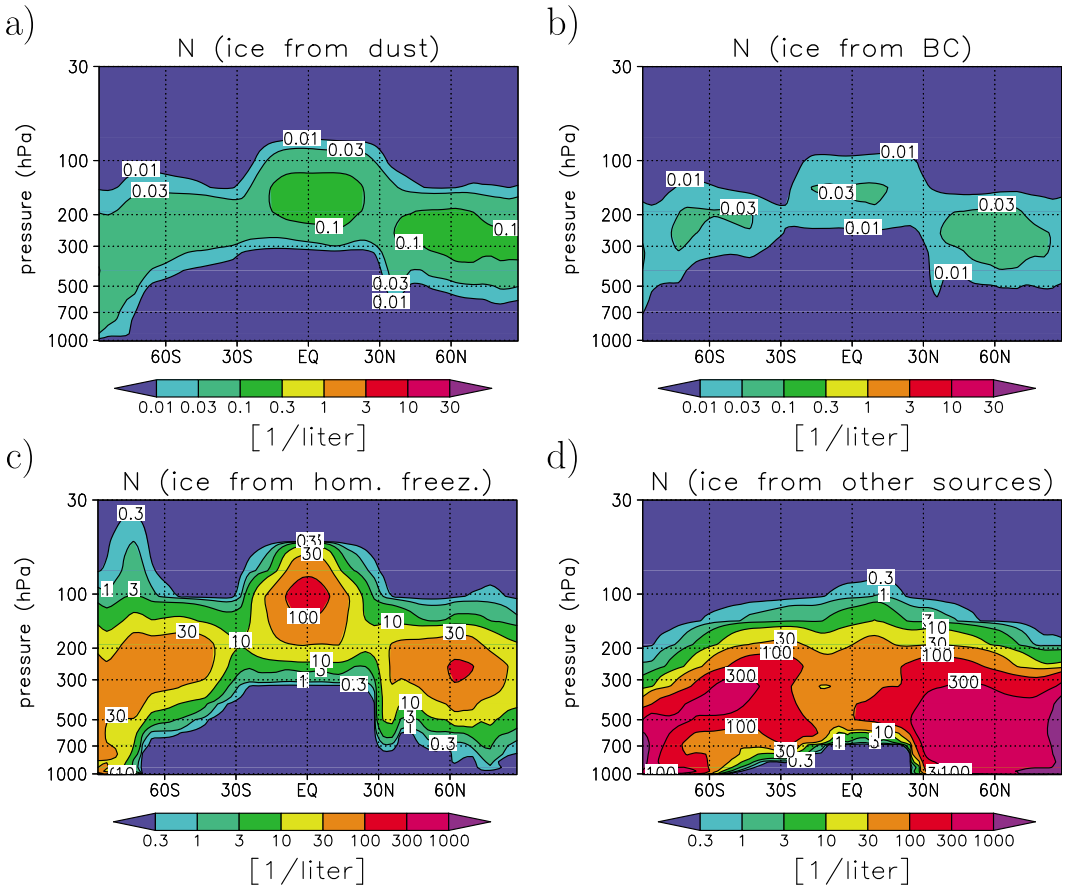

Figure 3. Vertical distributions of the zonally averaged annual mean crystal number concentration of ice formed by (a) heterogeneous nucleation on mineral dust (het-du mode), (b) heterogeneous nucleation on BC (het-bc mode), (c) homogeneous freezing of liquid aerosol (hom mode), and (d) other mechanisms (misc mode). Results are taken from simulation HETDB and represent 10 year averages. The concentrations were calculated as all-sky means by averaging over cloudy and cloud-free cases. Only clouds with a total ice water content larger than 0.5 mg/kg air were considered. Note the different scales in Figures 3a and 3b and Figures 3c and 3d.

fraction of the mineral dust IN might be activated to form the het-du mode. In this case, the het-bc mode will not form since the water vapor deposition on the few ice particles generated by mineral dust IN does not allow any further increase in relative humidity and, therefore, nucleation of poorer IN or liquid particles does not occur. If the cooling rate is large enough to activate all available dust IN, the het-du mode might interfere with the possible subsequent formation of the het-bc mode. If the impact of het-du on the relative humidity increase is large, the het-bc mode might not form at all or only a fraction of the available BC IN might be activated. This competition results in comparatively low ice particle number concentrations in the het-bc mode in simulation HETDB (Figure 3b). The het-bc particle number concentrations are about a factor of 3 larger in simulation HETBD (not shown) where the het-bc mode forms first, and therefore, the competition effect is absent.

[52] On average, cloud ice from mode hom formed by homogeneous freezing (Figure 3c) has the largest contribution to the total ice particle number in cold cirrus clouds. The zonal mean annual average number concentrations range from ~1 L^{-1} to values around 100 L^{-1} in areas of frequent cirrus occurrence (>10%), corresponding to average in-cloud concentrations of ~0.01–1 cm^{-3}. Figure 3d displays the ice particle concentration from the misc mode (other sources than freezing induced by IN or liquid aerosol at low temperatures). Large values in this mode mainly occur at lower altitudes and are therefore related to ice formation in low- and middle-level (supercooled, water-containing) clouds. Zonal mean annual average concentrations of up to 1 cm^{-3} are simulated, particularly at low levels, corresponding to mean in-cloud values of up to 10 cm^{-3}. Summing all modes results in mean total crystal number concentrations in the range of 0.01–1 cm^{-3} in areas of frequent cloud occurrence which correspond to mean in-cloud concentrations in the range of 0.1–10 cm^{-3}. These concentrations agree with the typical range of crystal number concentrations simulated by other global models [e.g., *Salzmann et al.*, 2010].

[53] The general features of the hom and misc modes and the total crystal number concentrations described above are similar in all simulations performed with the multiple mode ice scheme. However, differences occur because of varying the representation of heterogeneous nucleation, particularly

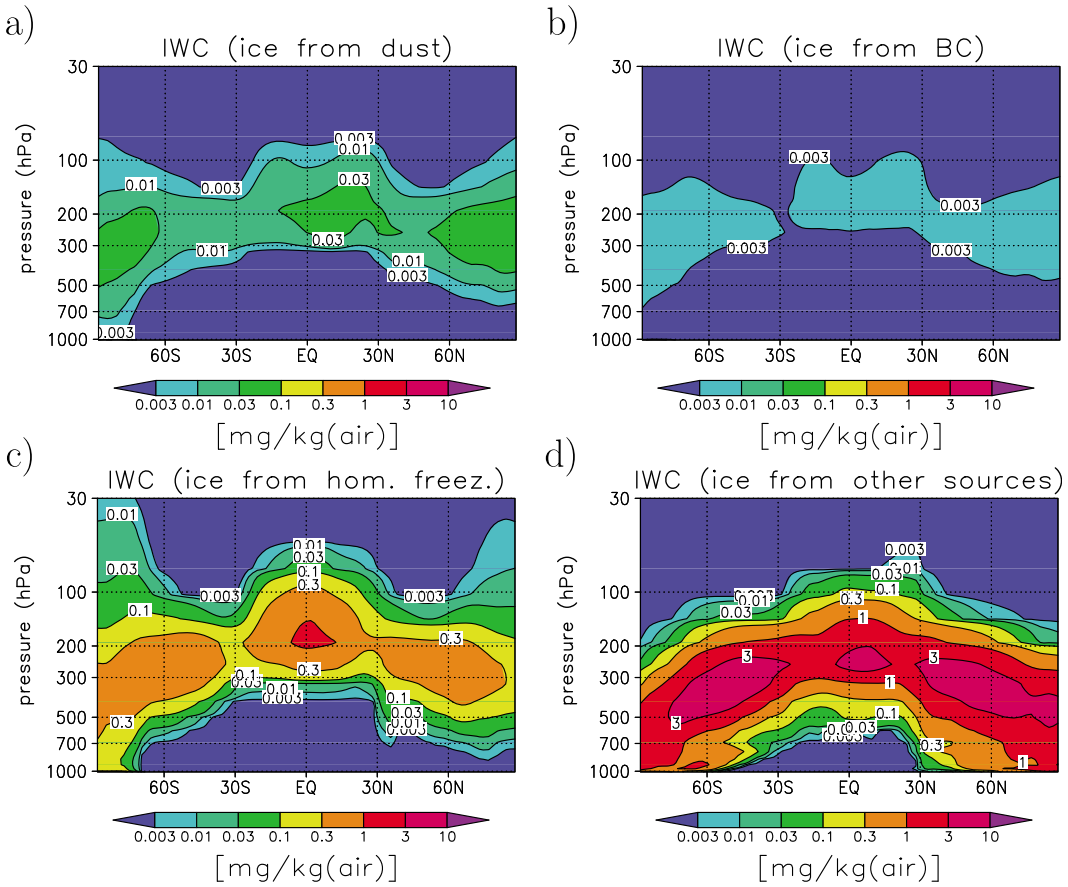

Figure 4. Same as Figure 3 but for the ice water content (IWC) of the different ice modes.

in the hom mode. These effects will be discussed separately in section 3.3.

3.1.3. Ice Water Content

[54] Vertical distributions of the zonal mean annual average ice water content of the different modes from experiment HETDB are displayed in Figure 4. The ice mode generated by heterogeneous ice nucleation on mineral dust (het-du, Figure 4a) shows typical zonal mean annual average ice water contents of 0.01–0.1 mg/kg air in the UTLS region. The mean ice water content of the het-bc mode (Figure 4b) is an order of magnitude smaller. As in the case of the ice particle number concentration, this can be due to the competition of the het-bc mode with the het-du mode. Another important reason can be the comparatively high RHI_{crit} value of 140% chosen for ice formation on BC in experiment HETDB. Since this value is close to the threshold for homogeneous freezing, the ice water content of the het-bc mode is frequently reduced because of competition with the hom mode for the water vapor available for ice deposition. This changes when a lower critical humidity for ice formation on BC is assumed. In simulation HETBD (not shown), the ice water content of the het-bc mode is larger compared to that of the het-du mode, particularly in the northern midlatitude (>45°N) troposphere, where BC particles are abundant. Because of the lower freezing threshold (120%), the het-bc mode can take up significantly more water from the gas phase, particularly at low updraft velocities where it forms considerably earlier than the het-du and hom modes.

[55] The mean ice water content of the mode resulting from homogeneous freezing in the UTLS lies in the range of 0.1–1 mg/kg air across all latitudes (hom mode from experiment HETDB; Figure 4c), exceeding the ice water content of the heterogeneous nucleation modes by an order of magnitude. On average, ice from other sources (misc mode; Figure 4d) contributes most to the total simulated ice water content, but only at lower altitudes (mostly at extratropical levels between 250 and 500 hPa and in the tropical upper troposphere around 250 hPa). Typical zonal mean annual average values range from 0.1 to 10 mg/kg air. As in the case of the particle number concentration, the general features of the ice water content of the hom and misc modes are similar in all simulations performed with the multiple mode ice scheme.

[56] The results discussed above indicate that ice from heterogeneous nucleation has a larger relative contribution to the total cloud ice water content than to the total cloud ice particle number concentration, particularly when RHI_{crit} is assumed to be distinctively lower than the threshold for homogeneous freezing. This confirms our conjecture that heterogeneous nucleation can generate comparatively large crystals in the het-du and het-bc modes which, consequently, can efficiently be removed by sedimentation and precipitation formation (section 2.2.3).

3.2. Comparison With Observations

3.2.1. Ice Crystal Number Concentration

[57] In situ observations by *Gayet et al.* [2004, 2006], *Hoyle et al.* [2005], *McFarquhar et al.* [2007], *Lawson et al.* [2008], and *Krämer et al.* [2009] suggest that ice crystal number concentrations in cirrus range between about 0.005 and several 10 cm^{-3}. Furthermore, these observations show that the highest concentrations are associated with the smallest ice crystal sizes. On the one hand, some of these data sets may be affected by shattering of larger ice particles on the instrument inlets [*McFarquhar et al.*, 2007], thereby creating artificially high number concentrations of pristine ice particles, so that the highest values may be regarded as overestimates. On the other hand, ice crystal number concentrations up to several 10 cm^{-3} can be expected from the theory of homogeneous freezing in the presence of mesoscale cooling rates that have been shown to control homogeneous ice formation in many locations [*Kärcher and Lohmann*, 2002; *Kärcher and Ström*, 2003; *Hoyle et al.*, 2005]. In this situation, it is difficult to compare global model results with in situ observations. However, our simulated range of in-cloud ice particle number concentrations (section 3.1.2) agrees with these data, given the uncertainty inherent in the measurements.

3.2.2. Ice Water Path and Effective Diameter

[58] Comparison of the GCM results with satellite-derived data sets is promising since long-term global satellite observations of ice cloud properties are available. However, a comparison with this kind of observational data is not straightforward as well and requires a very careful analysis of the satellite products and the model output as stressed, for instance, by *Kärcher et al.* [2009], *Waliser et al.* [2009], and *Hendricks et al.* [2010]. We apply a global observational data set of ice water path IWP and effective particle size D_{eff} of semitransparent cirrus (cirrus clouds in the solar optical thickness range between about 0.7 and 3.8). The data set was derived by *Rädel et al.* [2003] and *Stubenrauch et al.* [2004] using measurements by the TIROS-N Operational Vertical Sounder (TOVS) instruments aboard the Polar Orbiting Environmental Satellite NOAA10. Because of a high spectral resolution in the infrared, cirrus properties obtained from TOVS are especially reliable, day and night. The data applied here covers the 3 year period from 1988 to 1990. Figure 5 shows comparisons of model results with the TOVS data. Only cirrus clouds in the optical thickness range covered by TOVS were extracted from the model output as described by *Hendricks et al.* [2010]. The effective diameter of the simulated ice clouds was derived from the mean crystal size of the total ice population according to *Lohmann* [2002].

[59] Among the simulations including heterogeneous nucleation, experiment HETBD shows particularly large deviations in cirrus microphysical properties compared to experiment HOM (section 3.3). Hence, these two experiments are assumed to represent the range of cloud properties simulated with the new multiple mode ice scheme and are, therefore, compared to the observations. In addition, the simulation REF performed with the original cloud scheme is considered. Figure 5a shows the zonal mean annual average IWP as modeled in the simulations REF, HETBD, and HOM as well as the corresponding IWP from TOVS. The original model (REF) shows less IWP than TOVS. The IWP in the simulations increases when the modified cloud scheme is applied (HETBD, HOM) and the mean IWP values seem to be in better agreement with the TOVS data. In terms of global mean IWP the modified model and the TOVS data nearly match (Table 4). The effect of the modified cloud scheme on the representation of D_{eff} in semitransparent cirrus is shown in Figure 5b. Because of a reduction in crystal number concentration in the modified scheme, the mean values of D_{eff} are larger than in the reference scheme. This, on the one hand, results in a better agreement with TOVS in the tropics, where ice nuclei can be particularly efficient in perturbing cirrus [*Kärcher*, 2004]. On the other hand D_{eff} simulated with the new model considerably exceeds the observed values in the midlatitudes.

[60] The differences between the simulations HOM and HETBD are small with regard to IWP and D_{eff}. This indicates that the major differences to simulation REF do not result from the ice nuclei effects considered in HETBD but rather from other modifications, such as the changed formulation of sedimentation or the consideration of preexisting cloud ice in the ice nucleation parameterization. This, however, does not imply that IN effects are negligible in the simulations. The comparison discussed here focuses on semitransparent cirrus. Considering all high clouds (no restriction to specific optical thicknesses) reveals larger differences between HETBD and HOM particularly in the tropics (section 3.3).

[61] From the comparisons with TOVS we conclude that the new model performs well in simulating mean microphysical cloud features. However, in view of the uncertainties inherent in the retrieved D_{eff} and IWP, this conclusion should be carefully considered. Uncertainties of the observations can be as large as 30% and are mainly due to retrieval assumptions on particle shape and size distribution, temperature profiles, as well as horizontal and vertical heterogeneity [*Rädel et al.*, 2003; *Stubenrauch et al.*, 2004]. It should also be taken into account that the contribution of snow (precipitating ice particles with volume equivalent diameters larger than 200 μm, section 2.2.1) to the model IWP has not been considered, which could have caused a bias toward too small model IWP in the comparison.

3.2.3. Ice Water Content

[62] Global observations of the IWC in high clouds are provided by the Microwave Limb Sounder (MLS) on board the Aura satellite launched in July 2004 [*Waters et al.*, 2006]. To evaluate the IWC in the simulations presented here, we use MLS version 2.2 IWC data [*Wu et al.*, 2008; *Jiang et al.*, 2010]. We use 2 years of data from January 2005 to December 2006 screened for removing clear-sky residual noise and selecting significant cloud hits [*Wu et al.*, 2008]. Data of six pressure levels between 215 and 83 hPa are considered. Typical precisions of these data decrease from 0.6–1.3 to 0.06 mg/m^3 from 215 to 83 hPa. Because of saturation effects, large MLS IWC values can be particularly uncertain. The largest valid IWC amounts to 50 mg/m^3. The estimated measurement accuracy of the MLS IWC is a factor of 2.

[63] Figure 6a shows the zonal mean annual average vertical distribution of the MLS IWC between 215 and 83 hPa. The MLS data were transformed to the horizontal grid of the model to calculate averages. Corresponding

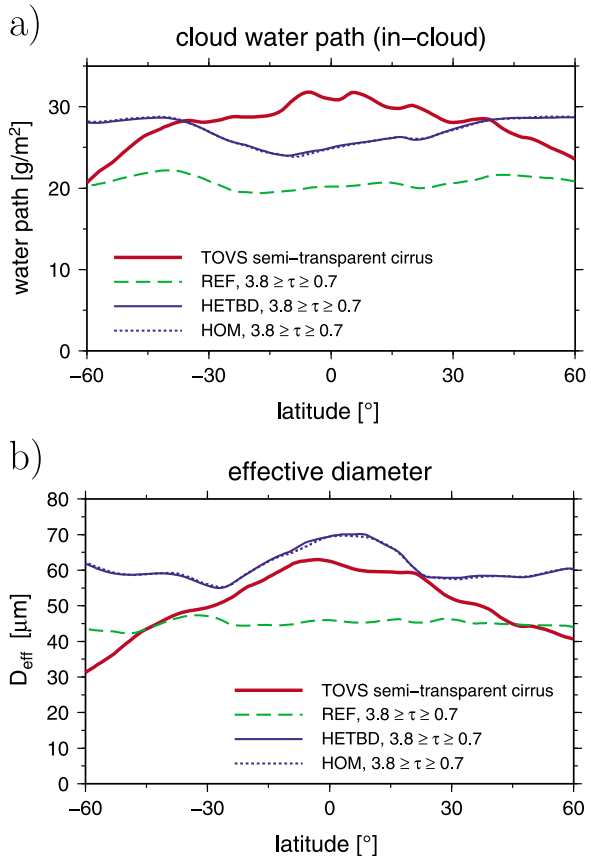

Figure 5. Zonal mean annual average (a) ice water path and (b) effective ice crystal diameter of semitransparent cirrus (high clouds with a solar optical thickness of $0.7 \leq \tau \leq 3.8$). The plots show data from the REF, HETBD, and HOM experiments as well as TIROS-N Operational Vertical Sounder (TOVS) satellite observations according to *Stubenrauch et al.* [2004]. The averages were calculated from in-cloud values only, which means that cloud-free areas were not considered.

model results are shown for simulations REF (Figure 6b) and HETBD (Figure 6c). The corresponding IWC distributions derived from the other simulations with the multiple-mode ice scheme (not shown) are very similar to the HETBD results. The observed and modeled vertical IWC distributions in the tropics are similar with regard to spatial patterns. The MLS IWC in the tropics, however, is about a factor of 2 larger than the modeled values, particularly at the lower levels between 215 and 150 hPa. A possible reason for this discrepancy is that the model IWC analyzed for the comparison only comprises ice in large-scale stratiform clouds. Snow (section 2.2.1) as well as ice in subgrid-scale convective clouds, which are handled by the convection parameterization, are not included in this analysis. However, it should be taken into account that the deviations between the model and the observations are on the order of the accuracy of the MLS data. Hence, also uncertainties of the observations can contribute to the discrepancies. At higher altitudes around the 100 hPa level, the model IWC in the simulation with the new ice scheme (HETBD) agrees better with the MLS data. Simulation REF still shows distinctively lower IWC than MLS. This can be due to the changes in the sedimentation formulation (section 2.2.5) which resulted in increased IWC compared to simulation REF at many locations.

[64] At midlatitudes, the model shows larger IWC than the MLS data. Particularly the HETBD simulation shows higher IWC at altitudes of low cloud occurrence frequency above 200 hPa. In addition to model uncertainties, for instance, in the representation of ice sedimentation, also uncertainties in the satellite data could contribute to this discrepancy. The IWC data from the CloudSat satellite which is now becoming available shows larger IWC values than MLS [*Waliser et al.*, 2009]. The mean IWC at midlatitudes above 200 hPa as suggested by the simulations is in better agreement with these data. Overall, the modeled vertical distribution qualitatively agrees with the satellite data, given the uncertainty associated with the various data sources.

3.2.4. Global Mean Cloud Properties

[65] Table 4 shows global mean values of cloud-related parameters from the model and different observational data sets. The total cloud cover is larger in simulations HETBD and HOM than in the reference run REF. This can be due to a less efficient ice sedimentation in the modified scheme and results in a better agreement with the observations. The total precipitation rate is in good agreement with the observations and changes only marginally with the cloud scheme. The modifications of the cloud scheme result in a slight decrease in the net cloud radiative forcing. The net cloud forcing changes mainly due to modifications of the short-wave forcing since for the crystal sizes regarded here, the short-wave forcing is more sensitive to changes in crystal size than the long-wave forcing [e.g., *Zhang et al.*, 1999]. The increase in IWP, which itself would lead to an increased short-wave cloud forcing, is overcompensated by the effect of the increase in D_{eff}. Compared to the REF simulation the net cloud forcing obtained with the new cloud scheme is in

Table 4. Global Annual Mean Cloud Properties From Simulations REF, HETBD, and HOM and From Observations (OBS)[a]

	REF	HETBD	HOM	OBS
IWP^{semi} (g m^{-2})	20.6	26.6	26.6	28.6
D_{eff}^{semi} (μm)	45.2	61.6	61.5	52.7
TCC (%)	60.1	66.1	66.2	62–67
P_{tot} (mm d^{-1})	2.81	2.81	2.79	2.74
SCF (W m^{-2})	−47.4	−44.6	−45.0	−47 to −50
LCF (W m^{-2})	28.4	28.4	28.7	22–30
CF (W m^{-2})	−19.0	−16.2	−16.3	−17 to −28

[a]The ice water path IWP^{semi} and effective ice particle diameter D_{eff}^{semi} were averaged over cloudy cases only. Because of observational constraints only semitransparent cirrus clouds (solar optical depth between 0.7 and 3.8) at latitudes between 60°S and 60°N have been considered. The observed values are taken from TIROS-N Operational Vertical Sounder (TOVS) satellite data [*Stubenrauch et al.*, 2004]. Total cloud cover (TCC) from ground-based measurements [*Hahn et al.*, 1994] and satellite observations from the International Satellite Cloud Climatology Project (ISCCP) [*Rossow and Schiffer*, 1999] and Moderate Resolution Imaging Spectroradiometer (MODIS) [*King et al.*, 2003] are considered. The observed total precipitation rate (P_{tot}) is taken from the Global Precipitation Climatology Project [*Adler et al.*, 2003]. The observational data for the short-wave (SCF), long-wave (LCF), and net cloud forcing (CF) are taken from the Earth Radiation Budget Experiment (ERBE) [*Kiehl and Trenberth*, 1997]. In addition, observations of LCF from TOVS [*Susskind et al.*, 1997; *Scott et al.*, 1999] and SCF from CERES [*Kim and Ramanathan*, 2008] are taken into account. See Table 3 for the simulations.

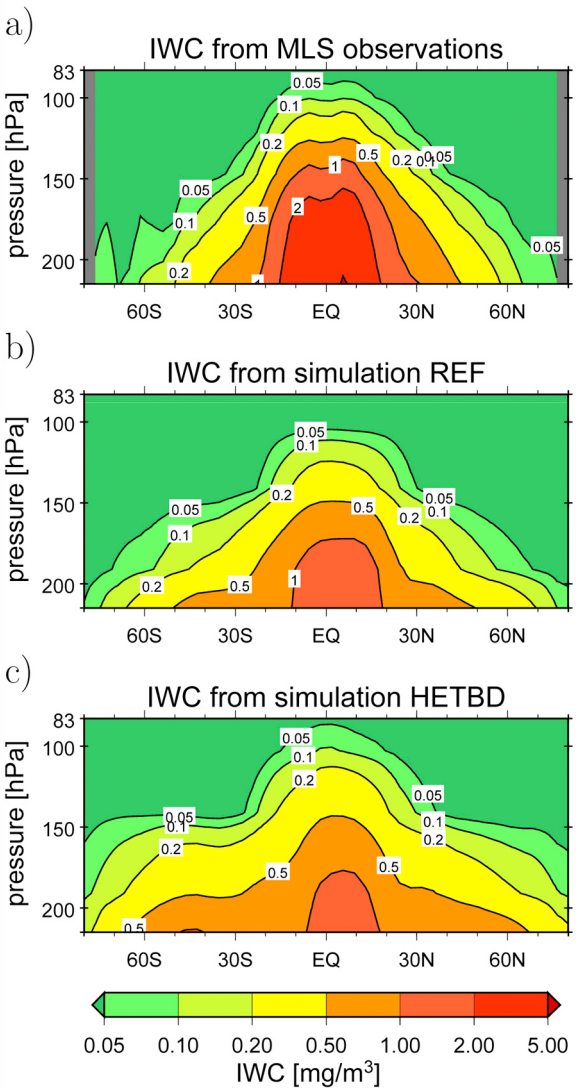

Figure 6. Vertical distributions of the zonally averaged annual mean ice water content from (a) Microwave Limb Sounder (MLS) observations, (b) simulation REF, and (c) simulation HETBD. The IWC was averaged over cloudy and cloud-free cases (all-sky means). MLS observations between January 2005 and December 2006 were considered. The model results represent 10 year averages.

worse agreement with the observations. However, it is still close to the observed range. While the differences in the global means induced by the new cloud scheme (differences between HOM or HETBD and REF) are generally significant, differences between the HETBD and HOM experiments mostly are small compared to the natural (interannual) variability of the respective mean cloud-related parameters. Hence, the quality of the representation of heterogeneous nucleation effects in the model cannot be evaluated with the data provided in Table 4.

3.2.5. Relative Humidity Over Ice

[66] The representation of ice supersaturation in the model applied here has been evaluated in earlier studies. *Lohmann and Kärcher* [2002] and also *Haag et al.* [2003] performed comparisons of RHI under cirrus conditions with MOZAIC (measurement of ozone and water vapor on Airbus in-service aircraft) data [*Gierens et al.*, 1999]. Frequency distributions of clear-sky RHI in simulations with ECHAM4 considering aerosol-induced cirrus formation only by homogeneous freezing were compared with the observational data. The comparison showed that the model is able to reproduce the quasi-exponential shape, which is characteristic for RHI frequency distributions in ice-supersaturated regions. Such comparisons could be performed also for the present simulations including the effects of heterogeneous nucleation. In these model runs, however, cirrus clouds generally form when RHI reaches the critical value RHI_{crit} assumed for the onset of heterogeneous nucleation. Hence, clear-sky RHI values larger than this threshold, assumed as 120% or 130% in the respective model runs, are suppressed. This implies a clear-sky frequency distribution of RHI similar to that derived from aircraft measurements in the Northern Hemisphere during the INCA field campaign [*Haag et al.*, 2003]. The MOZAIC data set covers both clear-sky and cloudy conditions [*Spichtinger et al.*, 2004]. Thus, RHI values above the heterogeneous freezing threshold frequently occur in this data set since RHI can further increase after heterogeneous nucleation when the cooling rate is sufficiently high. Hence, a comparison of the clear-sky frequency distribution gained from the model with the MOZAIC data would be meaningless. The option to compare all-sky RHI (including cloudy and cloud-free cases) is also not suitable since the large time steps in GCM often result in saturation ratios close to unity under cloudy conditions [*Wang and Penner*, 2010]. Also the use of satellite data for the evaluation of model RHI is not straightforward since these data sets either represent all-sky conditions or still contain signatures of thin cirrus [e.g., *Spichtinger et al.*, 2003; *Lohmann et al.*, 2008]. Hence, further long-term and large-scale in situ and satellite observational data on RHI for clear-sky conditions processed with highly sensitive cloud-clearing devices are required to enable a better evaluation of models.

3.3. Effects of Ice Nuclei on Cirrus

3.3.1. Effects on Ice Particle Number Concentration

[67] Figure 7a shows the zonal mean annual averages of the total ice crystal number concentration N_{ice} (sum over all modes) in the simulation HOM where heterogeneous ice formation at temperatures below T_{hom} is neglected and aerosol-induced cirrus formation is driven by homogeneous freezing only. Zonal mean crystal concentrations at cirrus levels reach values around 100 L^{-1} corresponding to mean in-cloud concentrations up to 1 cm^{-3}. Figures 7b–7d show the effects of IN from surface sources on the mean total crystal number concentration, revealed by simulations HETBD, HETDB, and HETD, respectively. The effects are derived from the differences between the respective simulation including heterogeneous nucleation and experiment HOM. Differences which are statistically significant at the 90% level of the Student's t test are highlighted in color. The results suggest that heterogeneous nucleation causes a reduction in the average N_{ice}. This was expected since heterogeneous ice formation diminishes the efficiency of homogeneous freezing. It either reduces the number of crystals formed during subsequent homogeneous freezing events or even prevents homogeneous freezing. Increases of the crystal

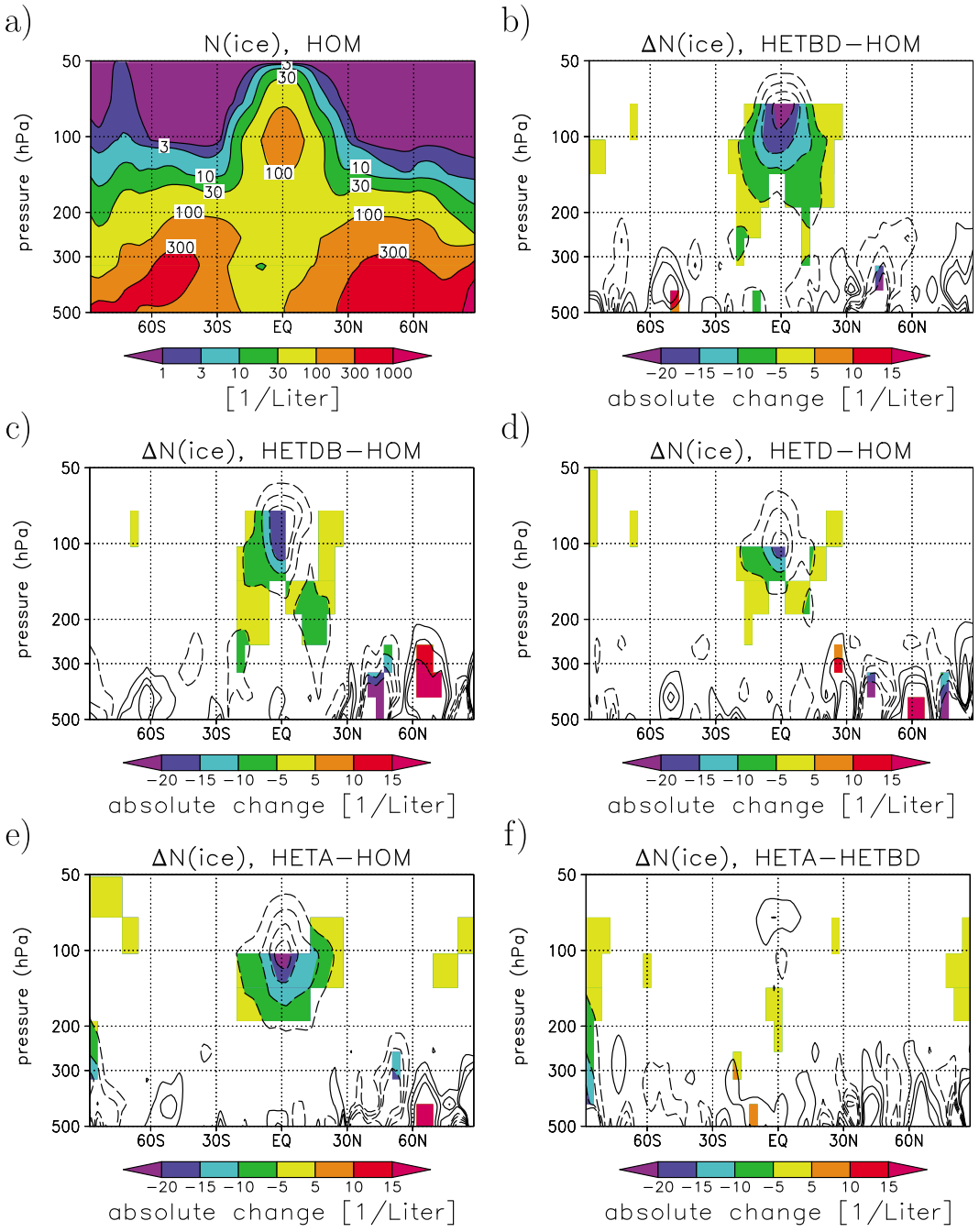

Figure 7. Same as Figure 3 but for (a) the total ice crystal number concentration (sum over all modes) in simulation HOM and the absolute change of the total crystal number concentration according to differences (b) HETBD minus HOM, (c) HETDB minus HOM, (d) HETD minus HOM, (e) HETA minus HOM, and (f) HETA minus HETBD. Changes significant at the 90% level of the Student's *t* test are highlighted in color. Note the different scales in Figures 7a and 7b–7f. The differences between simulations HETA and HETBD in the tropical upper troposphere and lowermost stratosphere (Figure 7f) are not significant and therefore cannot be interpreted as an effect of aviation. For a quantification of the change in crystal concentrations induced by BC from aircraft, see Figure 9b.

number possibly occurring at comparatively low cooling rates [*Kärcher et al.*, 2006] appear to be of secondary importance. Significant effects are simulated particularly in the tropical UTLS. The largest effect is simulated in experiment HETBD where the mean crystal concentration in the tropical UTLS is up to 20 L^{-1} lower than in experiment HOM. This corresponds to a relative reduction of about 20%. The effect is slightly smaller in simulations HETDB and HETD where heterogeneous nucleation on BC is assumed to occur at considerably higher supersaturations (HETDB) or is neglected at all (HETD). Maximum reductions in the average N_{ice} of about 15 L^{-1} are obtained in both cases. Simulation HETA is based

on the same assumptions as experiment HETBD, but heterogeneous nucleation on aircraft-generated BC is considered in addition. Compared to HETBD, the aviation BC effect does not change the magnitude of the total IN effect on N_{ice} (Figure 7e). However, it causes a vertical shift in the location of the maximum N_{ice} change to lower altitudes, where BC related to emissions along tropical flight routes is found more frequently [*Hendricks et al.*, 2004].

[68] The effects described above are mostly significant at the 90% level. However, less significant differences partly occur, particularly at higher altitudes. Nearly no significant differences in the average N_{ice} between experiments HETA and HETBD (Figure 7f) are found. The quantification of these signals is hampered by a considerably large variability of the crystal number concentration in cirrus caused, for instance, by the variability of mesoscale updraft velocities. In many cases this variability is larger than the IN effects simulated here. Because of low signal-to-noise ratios the effects cannot be quantified. Therefore, the increase in N_{ice} in the tropical UTLS calculated from the difference between experiments HETA and HETBD (Figure 7f) might be related to noise rather than heterogeneous nucleation on BC from aviation.

[69] These results show that the feasibility of analyzing the IN effects on N_{ice} by the comparison of different GCM simulations is limited. In particular, no significant signals can be quantified for the individual effects of BC from aviation (difference HETA minus HETBD) as well as for IN effects in general at midlatitudes. An analysis of the frequency of ice from homogeneous freezing, however, shows that such effects might not be negligible. We therefore discuss IN effects on homogeneous freezing in more detail in section 3.3.2 and describe the quantification of IN effects on N_{ice} by an alternative method in sections 3.3.3 and 3.3.4.

3.3.2. Effects on Homogeneous Freezing

[70] Figure 8a shows the frequency of occurrence of the ice mode hom formed by homogeneous freezing of liquid aerosol in experiment HOM. The frequency represents the annual and zonal mean grid box fractional coverage of clouds containing ice from homogeneous freezing. It ranges from about 20% up to 40% in areas of major cirrus occurrence. In the following, we analyze the potential of heterogeneous nucleation to perturb homogeneous freezing on the basis of experiments HETBD and HETA since the IN effects on N_{ice} are largest in these model runs (Figure 7). When heterogeneous nucleation is taken into account, the frequency of the hom mode is reduced significantly. Relative reductions of up to 10% occur when ice formation on IN from surface sources is taken into account (difference HETBD minus HOM; Figure 8b). The effect is particularly large at midlatitudes where no significant change of N_{ice} could be quantified. In the tropics only a small reduction of the frequency of the hom mode is simulated although large changes of N_{ice} are modeled (Figure 7b). This suggests that, in this area, heterogeneous nucleation rather reduces the crystal number formed by homogeneous freezing than shutting off homogeneous freezing entirely. Considering heterogeneous ice formation on BC from aviation causes an additional reduction of the frequency of hom at northern midlatitudes (Figure 8c). The relative reduction amounts to 5%–10% in the northern midlatitude UTLS compared to HETBD.

3.3.3. Alternative Quantification of Ice Nuclei Effects

[71] The frequency analysis discussed above suggests the potential for heterogeneous nucleation to affect N_{ice} even in areas where no significant N_{ice} change could be derived from the differences of the model experiments performed here. Heterogeneous nucleation results in ice modes characterized by particularly low crystal concentrations (Figure 3). Hence, distinctive reductions in the total ice crystal number concentration can be expected as a consequence of reductions in the occurrence frequency of homogeneous freezing caused by the presence of heterogeneous IN.

[72] The model assessment of IN effects on cirrus microphysical properties is complicated here by the noise inherent in the differences between the GCM simulations performed. As an alternative, we estimate the effects based on an analysis technique applied in single simulations. In these simulations, the ice formation parameterization [*Kärcher et al.*, 2006] is called twice, with different assumptions on ice nucleation. A standard call is used to drive the cloud module. A second call with modified assumptions on heterogeneous nucleation is used as a test call to assess potential changes in cloud properties due to differences in the nucleation process. This results in two different values of the total initial ice crystal number concentration N_{ini} supplied by the parameterization when new crystals are generated. In the following we denote the initial crystal number concentrations passed over to the cloud module as N_{ini}^{cloud} and the corresponding concentration from the test call as N_{ini}^{test}. Both quantities are kept as cloud attributes during the full lifetime of simulated cloud ice and are updated when additional crystals are generated during secondary nucleation events. The effect of changed ice nucleation assumptions on the current total ice crystal number is then estimated applying a simple scaling technique:

$$\Delta N_{ice} = \begin{cases} N_{ice}\left(\frac{N_{ini}^{test}}{N_{ini}^{cloud}} - 1\right), & \text{if } N_{ini}^{cloud} \neq 0, \\ 0, & \text{if } N_{ini}^{cloud} = 0. \end{cases} \quad (7)$$

Uncertainties are inherent in this method, particularly because of the neglect of microphysical changes caused by IN-induced differences in cloud aging. It is assumed that the relative change in ice particle number concentration described by equation (7) stays constant for the respective cloud, unless additional nucleation occurs. We apply the scaling method to the total ice population (sum over modes) present in modes het-du, het-bc, and hom. The misc mode is not considered since its crystal number has other sources than those represented by the *Kärcher et al.* [2006] parameterization and is not affected by the presence of IN during cirrus formation. Figure 9 shows the resulting zonal mean annual average change in ice crystal number concentration due to heterogeneous nucleation. We made the same assumptions on the IN freezing abilities as in experiments HETBD and HETA to maximize the effect. Effects of IN from surface sources (BC and mineral dust) are estimated from the simulation HOM including a test call of the ice nucleation parameterization considering heterogeneous nucleation as in simulation HETBD. The results shown in Figure 9a correspond to the difference between HETBD and HOM shown in Figure 7b. The scaling technique reveals maximum reductions in the mean ice crystal number concentration between about 10 and 30 L^{-1} in the tropics. The obtained signal is very

similar to the result from the difference between HETBD and HOM. Hence, the method seems to be robust enough to provide a good approximation of the effect.

3.3.4. Discussion of Ice Nuclei Effects on Cirrus

[73] No significant differences between the simulations HETBD and HOM were detected in the midlatitudes (Figure 7b). The scaling method, however, reveals a reduction in the zonal mean annual average midlatitude crystal concentration of about 1–5 L^{-1} (Figure 9a). This corresponds to relative reductions of 1%–10%, with the largest effects in the Northern Hemisphere where IN are particularly abundant. The midlatitude effect exhibits a marked seasonal variation (not shown) with largest reductions of more than 10% during summer and reductions of a few percent only during winter. This is mainly due to a higher availability of IN in the UTLS during summer caused by particularly efficient upward transport. IN concentrations at cirrus levels are larger in the midlatitudes than in the tropics (Figure 2). Their effect on N_{ice}, however, is largest in the tropics where reductions in the mean ice particle number concentration of up to 30 L^{-1} are simulated (Figure 9a), corresponding to relative reductions of up to 20%. This agrees with the study by *Kärcher* [2004] which suggests that even a small amount of efficient IN (1–10 L^{-1}) near the tropical tropopause has the potential of altering microphysical properties of cirrus. The effect was caused by assuming threshold relative humidities for heterogeneous ice nucleation lower than those required for homogeneous freezing. It also agrees with the results of *Penner et al.* [2009], who use an off-line approach based on ice nucleation parameterizations driven by precalculated meteorological fields and aerosol concentrations to quantify global aerosol effects on nucleated ice particle number concentration. Reductions in the mean ice crystal number concentration of several 10% induced by BC particles from anthropogenic sources at the Earth's surface where simulated for the tropical UT.

[74] In situ measurements by *Lawson et al.* [2008] in thin cirrus clouds close to the tropical tropopause indicate that ice crystal number concentrations can be small (<100 L^{-1}) under these conditions. *Jensen et al.* [2010] argued that such small concentrations probably cannot be caused by homogeneous freezing under these conditions and suggest that they could be related to having on the order of 50 L^{-1} effective ice nuclei (possibly composed of ammonium sulfate) nucleating ice at relatively low supersaturations. Although our simulations reveal that heterogeneous nucleation can have important effects in the tropical UTLS, homogeneous freezing frequently occurs and generates mean in-cloud ice crystal concentrations of several 100 L^{-1}. This, on the one hand, could be attributed to the modeled mean concentrations representing all types of ice clouds, including also thicker cirrus. On the other hand, the effect of heterogeneous nucleation in the simulations could be too small because of particular IN types not yet represented in

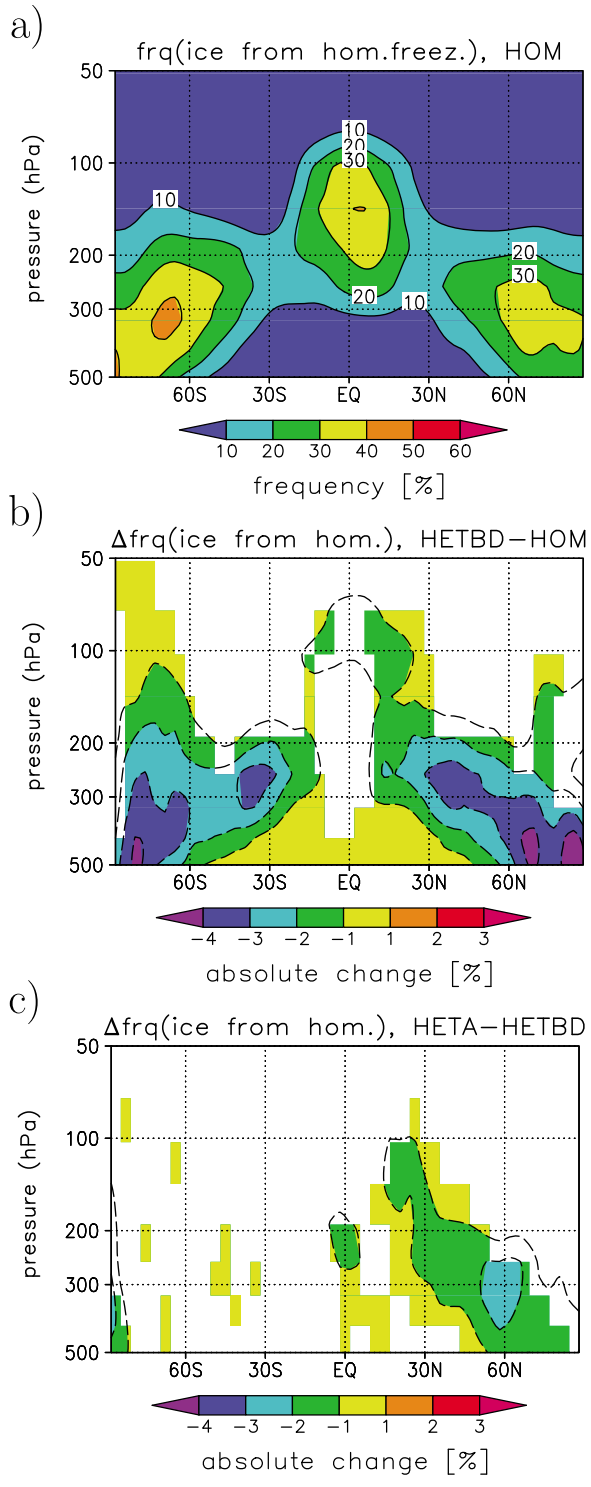

Figure 8. Vertical distributions of the zonally averaged annual mean (a) occurrence frequency of ice from homogeneous freezing of liquid aerosols (hom mode), (b) its absolute change due to heterogeneous nucleation on BC from surface sources and mineral dust particles (difference HETBD minus HOM), and (c) additional change due to ice formation on BC from aircraft (difference HETA minus HETBD). The occurrence frequency represents the annual and zonal mean grid box fractional coverage of clouds containing ice from homogeneous freezing. Only clouds with a total ice water content larger than 0.5 mg/kg air and a contribution of ice from homogeneous freezing larger than 1% of this threshold are considered. Changes significant at the 90% level of the Student's *t* test are highlighted in color. Note the different scales in Figure 8a and Figures 8b and 8c.

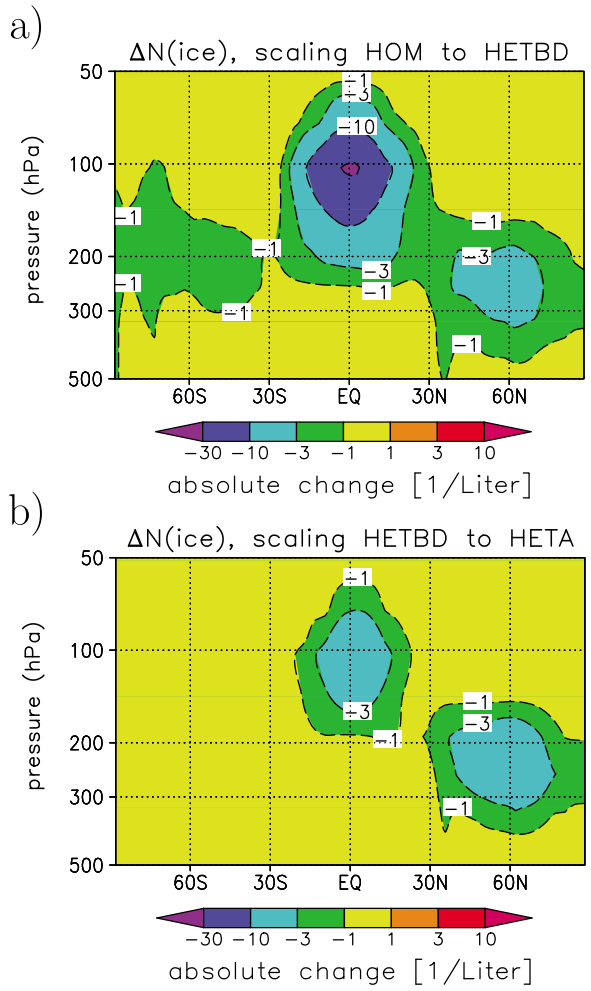

Figure 9. Same as Figure 7 but for the absolute change in crystal number concentration due to heterogeneous nucleation estimated by the scaling method. (a) Absolute change due to heterogeneous nucleation on BC from surface sources and mineral dust particles derived from scaling HOM to HETBD (corresponds to difference HETBD minus HOM) and (b) additional change due to heterogeneous nucleation on BC from aircraft derived from scaling HETBD to HETA (corresponds to difference HETA minus HETBD).

the model or because of too high cooling rates. Other in situ measurements by *Krämer et al.* [2009] also show very small ice crystal number concentrations in cold tropical cirrus clouds. Besides heterogeneous freezing, *Krämer et al.* [2009] suggest the suppression of homogeneous ice crystallization at low temperatures in highly viscous aqueous organic acid droplets [*Murray*, 2008] as a possible explanation for the low crystal numbers. Since this process is not yet considered in our model, homogeneous freezing could possibly generate too many particles at very low temperatures.

[75] Effects of IN resulting from BC emissions of aviation are estimated from the simulation HETBD including a test call of the ice nucleation parameterization considering heterogeneous nucleation as in simulation HETA. The result which corresponds to the difference between the simulations HETA and HETBD is shown in Figure 9b. Heterogeneous nucleation on aircraft-generated BC causes an additional reduction of the mean crystal number between about 1 and 5 L^{-1} at northern midlatitudes where high aviation activities lead to a considerable BC emission. This corresponds to an additional relative reduction in the mean ice crystal number concentration of up to 10%. A similar aviation effect in the tropics is simulated although concentrations of aircraft-generated BC are smaller here (Figure 2).

[76] The effect of BC from aviation on N_{ice} is smaller than in the study by *Hendricks et al.* [2005] where relative changes of the zonal mean annual average N_{ice} of up to 30% were simulated. An important reason for this difference is that smaller IN concentrations are considered in the present study. Only small fractions of the available BC and dust particles are assumed to form ice (section 2.3). *Hendricks et al.* [2005] assumed a scenario where all available BC and dust particles can act as IN (scenario 1). Alternatively they assumed that heterogeneous nucleation occurs on aircraft-generated BC only (scenario 2), still assuming that all BC particles from aviation can form ice. Another possible reason is the consideration of preexisting ice in the ice nucleation parameterization. This was neglected previously and probably limits increases in N_{ice} during secondary nucleation events. As in scenario 2 of *Hendricks et al.* [2005], aviation BC emissions cause a reduction of N_{ice} in the simulations performed here. This reveals that BC from aviation further diminishes the efficiency of homogeneous freezing, rather than increasing N_{ice} in a scenario which is already dominated by heterogeneous nucleation. A new feature of the present simulations, in comparison to that of *Hendricks et al.* [2005], is the aviation-induced decrease in N_{ice} in the tropics. Such an effect was also found by *Penner et al.* [2009]. In the *Hendricks et al.* [2005] study the aviation effect was restricted to midlatitudes since a high threshold IN concentration for the occurrence of heterogeneous freezing was assumed which was hardly reached in the tropics in scenario 2. In scenario 1 the aviation-induced IN perturbation probably was too small in the tropics to cause a detectable signal.

[77] The effect of heterogeneous ice nucleation on BC from aviation was also quantified in the GCM study by *Liu et al.* [2009]. The study reveals an increase in the zonal mean annual average ice crystal concentration at northern mid and high latitudes ranging between about 10 and 100 L^{-1} in a scenario where BC can form ice above critical relative humidities RHI_{crit} of 120%–130%. In these simulations, heterogeneous nucleation is assumed to occur on BC only and dust impacts are neglected. The aviation effect is reduced when RHI_{crit} is increased to 140% but still reaches values of more than 30 L^{-1}. These results are in contradiction to the small decrease of a few crystals per liter simulated in the present study. *Liu et al.* [2009] admit that the increase in N_{ice} obtained in their simulations indicates that heterogeneous nucleation dominates ice formation, particularly in the scenario where low values of RHI_{crit} were assumed. This is a similar result as obtained by *Hendricks et al.* [2005] for their scenario 1 where all BC and mineral dust particles were considered to serve as IN. A dominance of heterogeneous nucleation implies that heterogeneous ice formation controls the ice crystal number concentration and homogeneous freezing is of secondary importance. This, however, does not agree with inferences from in situ measurements [*Haag et al.*, 2003] which show that even in the polluted Northern

Hemisphere cirrus do not form exclusively on heterogeneous ice nuclei and homogeneous nucleation is of crucial importance. Furthermore, relative humidities observed from satellites often reach the homogeneous freezing threshold [*Kahn et al.*, 2009]. *Liu et al.* [2009] also quantified the effects of the total increase in BC from preindustrial to present-day conditions and found considerable cirrus perturbations. This analysis, however, might also be affected by dominance of heterogeneous nucleation. Potential reasons for this dominance in the *Liu et al.* [2009] results as, for instance, too low maximum RHI values, are discussed by *Penner et al.* [2009] who performed off-line calculations with the ice nucleation parameterizations applied by *Liu et al.* [2009]. In these calculations, the dominance of heterogeneous nucleation is reduced and occurs only at lower levels (below about 200 hPa), predominantly in the Northern Hemisphere.

[78] Along with the perturbations of N_{ice} described above, the consideration of heterogeneous nucleation in the present study also affects the ice water content. The simulations suggest significant reductions of the ice water content when heterogeneous nucleation on IN from surface sources is considered (not shown). The effect particularly occurs in the tropics where also significant changes of N_{ice} are simulated. Relative reductions of up to 10%, in terms of zonal mean annual averages, are obtained when simulation HETBD is compared to simulation HOM. No significant changes of the ice water content due to BC from aviation could be detected. The quantification of such an effect as well as the detection of possible ice water content changes in the midlatitudes due to IN from surface sources might suffer from too low signal-to-noise ratios and should be the subject of a more refined analysis in future studies. However, the consideration of IN causes significant reductions in the UTLS water vapor concentration in the tropics and the midlatitudes. Reductions in the zonal mean annual average water vapor mixing ratio of up to 5% occur because of the consideration of IN in simulation HETBD (difference between HETBD and HOM). The model runs performed here suggest that the cloud occurrence frequency is less sensitive to the microphysical perturbations induced by IN. Significant changes rarely occur. However, also this quantity should be a subject of future analysis.

4. Conclusions and Future Directions

[79] The novel multiple mode ice microphysical scheme applied in the ECHAM GCM allows the quantification of the individual microphysical properties of cloud ice formed by different heterogeneous ice nucleation pathways (specifically those triggered by mineral dust and black carbon ice nuclei at cirrus temperatures), by homogeneous freezing of supercooled aerosols and from other sources (glaciation of supercooled water clouds, deep convective outflow, ice formation by cloud droplet–snow collisions, and heterogeneous deposition-condensation nucleation at warmer temperatures). The competition of these modes for available water is realized in a physical parameterization scheme describing ice formation, which additionally considers the effect of preexisting ice on the ice nucleation process.

[80] Our simulations reveal specific regional and global climatological characteristics of ice formed on different aerosol types. Ice formed at low temperatures in the UTLS by homogeneous freezing of liquid aerosol has very large contributions to the mean ice crystal number concentration and ice water content. The ice modes formed by heterogeneous nucleation on a limited number of mineral dust and black carbon IN particles modulate the simulated cirrus properties. On average, these heterogeneous nucleation modes have small contributions to the total ice particle number concentration. Because of these small number concentrations, ice particles formed by heterogeneous nucleation can grow to comparatively large sizes, which implies that they can be subject to efficient sedimentation and precipitation formation. This is consistent with larger mean contributions of ice from heterogeneous nucleation to the total ice water content than to the total number concentration in our simulations.

[81] The global effects of ice nuclei on cirrus clouds were quantified by a set of simulation scenarios assuming various critical relative humidity thresholds at which ice can form heterogeneously as well as fixed ice active fractions of mineral dust and black carbon particles. The choices of both parameters were guided by field and laboratory studies. We note, however, that current observational data sets do not provide sufficient information to fully constrain these parameters. Our results suggest reductions in the zonal mean annual average cirrus ice particle number concentrations induced by heterogeneous ice nuclei in cirrus levels. The largest reductions of up to 20% predicted by our simulations occur in the tropics when ice nuclei related to black carbon from surface sources and mineral dust are assumed to form ice above critical relative humidity thresholds of 120% and 130% over ice, respectively. The mean reductions amount to 1%–10% in midlatitudes, with largest changes in the Northern Hemisphere where the abundance of ice nuclei is high. Coincident with the largest changes in ice particle number, reductions in the mean ice water content of up to 10% are simulated in the tropical regions. This is likely a consequence of efficient sedimentation and precipitation of large ice particles generated by heterogeneous nucleation and leads to a decrease in UTLS water vapor concentrations. The zonal mean annual average water vapor mixing ratio is reduced by up to 5% in the tropical and midlatitude UTLS. The comparatively large effects of ice nuclei on tropical cirrus as simulated here suggest that thin tropopause cirrus clouds, which frequently occur in the tropics, are particularly susceptible to perturbations induced by ice nuclei.

[82] Regarding large-scale aircraft soot effects on cirrus, an additional reduction in the UTLS ice crystal number concentration is simulated when heterogeneous ice formation on jet engine-generated black carbon particles is included in the simulations. The decrease in the zonal mean annual average ice crystal number concentration amounts to 1%–10% at northern midlatitudes and in the tropics. These estimates are based on the assumption of a rather high ice active fraction of 10% and a rather low critical relative humidity threshold of 120% for heterogeneous nucleation on aircraft-generated soot particles. In the tropics, a relevant aviation effect is simulated, although the contribution to the black carbon budget from aviation is small. This is a new result compared to our earlier studies [*Hendricks et al.*, 2005] which suggested that aviation soot effects are restricted to northern midlatitudes. An additional important difference to the earlier studies is that the cirrus perturbations induced by soot from aviation are distinctively smaller in the present

simulations. Compared to another global model study by *Liu et al.* [2009], the simulations presented here also suggest a smaller aviation soot effect on cirrus ice crystal number concentration, with opposite sign. While aviation soot causes a reduction in the mean crystal number concentration in our simulations, *Liu et al.* [2009] suggest an increase in crystal number. These differences could be due to a smaller availability of active ice nuclei assumed in the present study or differences in the representation of cooling rates.

[83] The new multiple ice mode scheme applied here has also been used to analyze the frequency of occurrence of cirrus clouds formed by specific ice modes. IN-induced decreases in the mean occurrence frequency of ice from homogeneous freezing of liquid aerosols reveal that the competition with heterogeneous nucleation can prevent homogeneous freezing from occurring, particularly in the midlatitudes, where relative frequency reductions of up to 10% are simulated. In the tropics, the reduction is small, which indicates that the large reductions in the mean ice particle concentration induced by heterogeneous nucleation there are mainly caused by a decrease of the number of ice particles formed by homogeneous freezing (and not by complete inhibition of homogeneous freezing).

[84] The results of the present study demonstrate that ice nuclei can affect cirrus clouds globally by inducing specific regional perturbations to the cloud ice particle number and ice water content. Future studies should focus on the radiative and climatic impacts of mineral dust and black carbon ice nuclei. Recent laboratory studies reveal that homogeneous freezing can be suppressed at low temperatures in highly viscous aqueous organic acid droplets [*Murray*, 2008]. It was further shown that glassy organic aerosols can possibly act as nuclei for heterogeneous ice nucleation at low temperatures in the tropical UTLS [*Murray et al.*, 2010]. Recent field measurements indicate that significant amounts of internally mixed sulfate-organic particles are available in the tropical tropopause layer and could be involved in cirrus formation [*Froyd et al.*, 2009, 2010]. Hence, possible effects of organic aerosol compounds on tropical cirrus warrant attention in global model studies. Other laboratory studies indicate a potential for heterogeneous ice nucleation on crystalline ammonium sulfate particles [e.g., *Abbatt et al.*, 2006; *Wise et al.*, 2009; *Baustian et al.*, 2010]. Hence, also the potential of such aerosol particles for changing global cirrus properties could be investigated by means of further global modeling.

[85] There are several issues that currently prevent a robust quantification of the global effects of ice nuclei on clouds and precipitation. The level of understanding of heterogeneous ice nucleation is poor, in part owing to the lack of data taken in the troposphere and the lack of physical theory to describe ice formation rates of various nucleation modes accurately. In situ measurements better constraining the relevant parameters of ice nuclei as well as a better understanding of the interplay between small-scale variability in supersaturation and ice nucleation are regarded as crucial steps to make headway in evaluating the role of ice nuclei in the atmosphere-climate system. Supported by theory and cloud-resolving simulations, such information may help to improve the simulation of the global effects of ice nuclei on mixed-phase clouds and pure ice clouds via suitable microphysical parameterizations.

[86] With reference to ice phase processes, cloud schemes in large-scale models need to be modified in order to reconcile the physical treatments of cloud fraction, ice supersaturation and ice microphysics [*Kärcher and Burkhardt*, 2008]. Traditional approaches treat liquid clouds and cirrus on the basis of the same physical assumptions, although observations demonstrate that significant differences exist between these cloud types. These differences necessitate a special treatment of pure ice clouds. In this context, we recall the crucial importance of improved vertical velocity estimates for simulating ice nuclei effects [e.g., *Joos et al.*, 2009]. Large-scale vertical wind speeds must not be used to drive our ice nucleation parameterization, because this would lead to a serious underestimate of the number of ice crystals formed by homogeneous freezing and tend to overemphasize the effects of ice nuclei in the cirrus formation process [*Kärcher and Ström*, 2003]. Higher vertical wind speeds and associated temperature changes lessen the effects of ice nuclei. In the absence of a consistent, model-based method to estimate the entire subgrid variability of the vertical wind field relevant for ice nucleation, we use ECHAMs turbulent kinetic energy to calculate an unresolved vertical wind component [*Lohmann and Kärcher*, 2002], yielding realistic ice crystal concentrations. Clearly, more efforts must be directed toward solving these issues. To evaluate refined large-scale model representations of cirrus microphysics, more long-term global observational data on ice microphysical parameters with reduced uncertainties are required. Finally, global models need to predict the state of mixing of ice-nucleating aerosol particles, besides number and size, as the mixing state is one important parameter controlling the ice nucleation activity. This requires the coupling of global atmospheric models with interactive, detailed aerosol modules [e.g., *Aquila et al.*, 2011].

[87] **Acknowledgments.** We particularly thank Ulrike Burkhardt for helpful comments on the manuscript and Klaus Gierens, Michael Ponater, Robert Sausen, Ulrich Schumann, and Ingo Sölch for valuable discussions. We thank the reviewers of the manuscript, who helped to identify areas that needed to be improved. We would like to acknowledge Claudia J. Stubenrauch (Laboratoire de Météorologie Dynamique, CNRS/IPSL) for providing the TOVS data. We thank Jonathan H. Jiang (Jet Propulsion Laboratory, California Institute of Technology) for providing the MLS data and performing the data quality screening. This research was performed within the DLR project "Climate-compatible air transport system" (CATS) and the Helmholtz Gemeinschaft Deutscher Forschungszentren (HGF) Virtual Institute Aerosol-Cloud-Interactions (VI-ACI). The model runs were performed at the German Climate Computing Centre (DKRZ, Hamburg, Germany).

References

Abbatt, J. P. D., S. Benz, D. J. Cziczo, Z. Kanji, U. Lohmann, and O. Möhler (2006), Solid ammonium sulfate aerosols as ice nuclei: A pathway for cirrus cloud formation, *Science*, *313*, 1770–1773.

Adler, R. F., et al. (2003), The version-2 global precipitation climatology project (GPCP) monthly precipitation analysis (1979-present), *J. Hydrometeorol.*, *4*, 1147–1167.

Aquila, V., et al. (2011), MADE-in: A new aerosol microphysics submodel for global simulation of insoluble particles and their mixing state, *Geosci. Model Dev.*, *4*, 325–355.

Archuleta, C. A., P. J. DeMott, and S. M. Kreidenweis (2005), Ice nucleation by surrogates for atmospheric mineral dusts and mineral dust/sulfate particles at cirrus temperatures, *Atmos. Chem. Phys.*, *5*, 2617–2634.

Barahona, D., and A. Nenes (2009), Parameterizing the competition between homogeneous and heterogeneous freezing in ice cloud formation—Polydisperse ice nuclei, *Atmos. Chem. Phys.*, *9*, 5933–5948.

Baustian, K. J., M. E. Wise, and M. A. Tolbert (2010), Depositional ice nucleation on solid ammonium sulfate and glutaric acid particles, *Atmos. Chem. Phys.*, *10*, 2307–2317.

Brasseur, G. P., and M. Gupta (2010), Impact of aviation on climate: Research priorities, *Bull. Am. Meteorol. Soc.*, *91*, 461–463.

Burkhardt, U., B. Kärcher, and U. Schumann (2010), Global modeling of the contrail and contrail cirrus climate impact, *Bull. Am. Meteorol. Soc.*, *91*, 479–483.

Cantrell, W., and A. J. Heymsfield (2005), Production of ice in tropospheric clouds: A review, *Bull. Am. Meteorol. Soc.*, *86*, 795–807.

Chen, Y., S. M. Kreidenweis, L. M. McInnes, D. C. Rogers, and P. J. DeMott (1998), Single particle analysis of ice nucleating aerosols in the upper troposphere and lower stratosphere, *Geophys. Res. Lett.*, *25*, 1391–1394.

Cziczo, D. J., K. D. Froyd, S. J. Gallavardin, O. Moehler, S. Benz, H. Saathoff, and D. M. Murphy (2009a), Deactivation of ice nuclei due to atmospherically relevant surface coatings, *Environ. Res. Lett.*, *4*, 044013, doi:10.1088/1748-9326/4/4/044013.

Cziczo, D. J., et al. (2009b), Inadvertent climate modification due to anthropogenic lead, *Nat. Geosci.*, *2*, 333–336.

DeMott, P. J., D. C. Rogers, and S. M. Kreidenweis (1997), The susceptibility of ice formation in upper tropospheric clouds to insoluble aerosol components, *J. Geophys. Res.*, *102*, 19,575–19,584.

DeMott, P. J., Y. Chen, S. M. Kreidenweis, D. C. Rogers, and D. E. Sherman (1999), Ice formation by black carbon particles, *Geophys. Res. Lett.*, *26*, 2429–2432.

DeMott, P. J., D. J. Cziczo, A. J. Prenni, D. M. Murphy, S. M. Kreidenweis, D. S. Thomson, and R. Borys (2003), Measurements of the concentration and composition of nuclei for cirrus formation, *Proc. Natl. Acad. Sci. U. S. A.*, *100*, 14,655–14,660.

DeMott, P. J., M. D. Petters, A. J. Prenni, C. M. Carrico, S. M. Kreidenweis, J. L. Collett Jr., and H. Moosmüller (2009), Ice nucleation behavior of biomass combustion particles at cirrus temperatures, *J. Geophys. Res.*, *114*, D16205, doi:10.1029/2009JD012036.

DeMott, P. J., A. J. Prenni, X. Liu, S. M. Kreidenweis, M. D. Petters, C. H. Twohy, M. S. Richardson, T. Eidhammer, and D. C. Rogers (2010), Predicting global atmospheric ice nuclei distributions and their impacts on climate, *Proc. Natl. Acad. Sci. U. S. A.*, *107*, 11,207–11,222.

Döpelheuer, A. (2002), Anwendungsorientierte Verfahren zur Bestimmung von CO, HC und Ruß aus Luftfahrttriebwerken, *Rep. 2002-10*, Dtsch. Zent. für Luft- und Raumfahrt, Cologne, Germany.

Feichter, J., E. Kjellström, H. Rodhe, F. Dentener, J. Lelieveld, and G. J. Roelofs (1996), Simulation of the tropospheric sulfur cycle in a global climate model, *Atmos. Environ.*, *30*, 1693–1707.

Field, P. R. (2000), Bimodal ice spectra in frontal clouds, *Q. J. R. Meteorol. Soc.*, *126*, 379–392.

Field, P. R., and A. J. Heymsfield (2003), Aggregation and scaling of ice crystal size distributions, *J. Atmos. Sci.*, *60*, 544–560.

Field, P. R., O. Möhler, P. Connolly, M. Krämer, R. Cotton, A. J. Heymsfield, H. Saathoff, and M. Schnaiter (2006), Some ice nucleation characteristics of Asian and Saharan desert dust, *Atmos. Chem. Phys.*, *6*, 2991–3006.

Forster, P., et al. (2007), Changes in atmospheric constituents and in radiative forcing, in *Climate Change* 2007*: The Physical Science Basis, Contribution of Working Group I to the Fourth Assessment Report of the Intergovernmental Panel on Climate Change*, edited by S. Solomon et al., pp. 129–234, Cambridge Univ. Press, Cambridge, U. K.

Froyd, K. D., D. M. Murphy, T. J. Sanford, D. S. Thomson, J. C. Wilson, L. Pfister, and L. Lait (2009), Aerosol composition of the tropical upper troposphere, *Atmos. Chem. Phys.*, *9*, 4363–4385.

Froyd, K. D., D. M. Murphy, P. Lawson, D. Baumgardner, and R. L. Herman (2010), Aerosols that form subvisible cirrus at the tropical tropopause, *Atmos. Chem. Phys.*, *10*, 209–218.

Gayet, J.-F., J. Ovarlez, V. Shcherbakov, J. Ström, U. Schumann, A. Minikin, F. Auriol, A. Petzold, and M. Monier (2004), Cirrus cloud microphysical and optical properties at southern and northern midlatitudes during the INCA experiment, *J. Geophys. Res.*, *109*, D20206, doi:10.1029/2004JD004803.

Gayet, J.-F., V. Shcherbakov, H. Mannstein, A. Minikin, U. Schumann, J. Ström, A. Petzold, J. Ovarlez, and F. Immler (2006), Microphysical and optical properties of midlatitude cirrus clouds observed in the Southern Hemisphere during INCA, *Q. J. R. Meteorol. Soc.*, *132*, 2719–2748.

Gettelman, A., X. Liu, S. J. Ghan, H. Morrison, S. Park, A. J. Conley, S. A. Klein, J. Boyle, D. L. Mitchell, and J.-L. F. Li (2010), Global simulations of ice nucleation and ice supersaturation with an improved cloud scheme in the Community Atmosphere Model, *J. Geophys. Res.*, *115*, D18216, doi:10.1029/2009JD013797.

Gierens, K. (2003), On the transition between heterogeneous and homogeneous freezing, *Atmos. Chem. Phys.*, *3*, 437–446.

Gierens, K., U. Schumann, M. Helten, H. Smit, and A. Marenco (1999), A distribution law for relative humidity in the upper troposphere and lower stratosphere derived from three years of MOZAIC measurements, *Ann. Geophys.*, *17*, 1218–1226.

Haag, W., B. Kärcher, J. Ström, A. Minikin, U. Lohmann, J. Ovarlez, and A. Stohl (2003), Freezing thresholds and cirrus cloud formation mechanisms inferred from in situ measurements of relative humidity, *Atmos. Chem. Phys.*, *3*, 1791–1806.

Hahn, C. J., S. G. Warren, and J. London (1994), Climatological data for clouds over the globe from surface observations, 1982-1991: The total cloud edition, *Tech. Rep. ORNL/CDIAC-72 NDP-026A*, Oak Ridge Natl. Lab., Oak Ridge, Tenn.

Heintzenberg, J., and R. J. Charlson (2009), Introduction, in *Clouds in the Perturbed Climate System: Their Relationship to Energy Balance, Atmospheric Dynamics, and Precipitation*, edited by J. Heintzenberg and R. J. Charlson, pp. 1–16, MIT Press, Cambridge, Mass.

Hendricks, J., B. Kärcher, A. Döpelheuer, J. Feichter, U. Lohmann, and D. Baumgardner (2004), Simulating the global atmospheric black carbon cycle: A revisit to the contribution of aircraft emissions, *Atmos. Chem. Phys.*, *4*, 2521–2541.

Hendricks, J., B. Kärcher, U. Lohmann, and M. Ponater (2005), Do aircraft black carbon emissions affect cirrus clouds on the global scale?, *Geophys. Res. Lett.*, *32*, L12814, doi:10.1029/2005GL022740.

Hendricks, J., A. Falb, C. J. Stubenrauch, and C. Emde (2010), A method for comparing properties of cirrus clouds in global climate models with those retrieved from IR sounder satellite observations, *Meteorol. Z.*, *19*, 577–589.

Hess, M., P. Koepke, and I. Schult (1998), Optical properties of aerosols and clouds: The software package OPAC, *Bull. Am. Meteorol. Soc.*, *79*, 831–844.

Heymsfield, A. J. (1977), Precipitation development in stratiform ice clouds: A microphysical and dynamical study, *J. Atmos. Sci.*, *34*, 367–381.

Heymsfield, A. J., and R. M. Sabin (1989), Cirrus crystal nucleation by homogeneous freezing of solution droplets, *J. Atmos. Sci.*, *46*, 2252–2264.

Heymsfield, A. J., A. Bansemer, and C. H. Twohy (2007), Refinements to ice particle mass dimensional and terminal velocity relationships for ice clouds. Part I: Temperature dependence, *J. Atmos. Sci.*, *64*, 1047–1067.

Hoyle, C. R., B. P. Luo, and T. Peter (2005), The origin of high ice crystal number densities in cirrus clouds, *J. Atmos. Sci.*, *62*, 2568–2579.

Jensen, E. J., L. Pfister, T.-P. Bui, P. Lawson, and D. Baumgardner (2010), Ice nucleation and cloud microphysical properties in tropical tropopause layer cirrus, *Atmos. Chem. Phys.*, *10*, 1369–1384.

Jiang, J. H., et al. (2010), Five year (2004–2009) observations of upper tropospheric water vapor and cloud ice from MLS and comparisons with GEOS-5 analyses, *J. Geophys. Res.*, *115*, D15103, doi:10.1029/2009JD013256.

Joos, H., P. Spichtinger, and U. Lohmann (2009), Orographic cirrus in a future climate, *Atmos. Chem. Phys.*, *9*, 7825–7845.

Kahn, B. H., A. Gettelman, E. J. Fetzer, A. Eldering, and C. K. Liang (2009), Cloudy and clear-sky relative humidity in the upper troposphere observed by the A-train, *J. Geophys. Res.*, *114*, D00H02, doi:10.1029/2009JD011738.

Kajikawa, M., and A. J. Heymsfield (1989), Aggregation of ice crystals in cirrus, *J. Atmos. Sci.*, *46*, 3108–3121.

Kärcher, B. (2004), Cirrus clouds in the tropical tropopause layer: Role of heterogeneous ice nuclei, *Geophys. Res. Lett.*, *31*, L12101, doi:10.1029/2004GL019774.

Kärcher, B., and U. Burkhardt (2008), A cirrus cloud scheme for general circulation models, *Q. J. R. Meteorol. Soc.*, *134*, 1439–1461.

Kärcher, B., and U. Lohmann (2002), A parameterization of cirrus cloud formation: Homogeneous freezing including effects of aerosol size, *J. Geophys. Res.*, *107*(D23), 4698, doi:10.1029/2001JD001429.

Kärcher, B., and U. Lohmann (2003), A parameterization of cirrus cloud formation: Heterogeneous freezing, *J. Geophys. Res.*, *108*(D14), 4402, doi:10.1029/2002JD003220.

Kärcher, B., and P. Spichtinger (2009), Cloud-controlling factors of cirrus, in *Clouds in the Perturbed Climate System: Their Relationship to Energy Balance, Atmospheric Dynamics, and Precipitation*, edited by J. Heintzenberg and R. J. Charlson, pp. 173–196, MIT Press, Cambridge, Mass.

Kärcher, B., and J. Ström (2003), The roles of dynamical variability and aerosols in cirrus cloud formation, *Atmos. Chem. Phys.*, *3*, 823–838.

Kärcher, B., J. Hendricks, and U. Lohmann (2006), Physically based parameterization of cirrus cloud formation for use in global atmospheric models, *J. Geophys. Res.*, *111*, D01205, doi:10.1029/2005JD006219.

Kärcher, B., O. Möhler, P. J. DeMott, S. Pechtl, and F. Yu (2007), Insights into the role of soot aerosols in cirrus cloud formation, *Atmos. Chem. Phys.*, *7*, 4203–4227.

Kärcher, B., U. Burkhardt, S. Unterstrasser, and P. Minnis (2009), Factors controlling contrail cirrus optical depth, *Atmos. Chem. Phys.*, *9*, 6229–6254.

Kiehl, J. T., and K. E. Trenberth (1997), Earth's annual global mean energy budget, *Bull. Am. Meteorol. Soc.*, *78*, 197–208.
Kim, D., and V. Ramanathan (2008), Solar radiation budget and radiative forcing due to aerosols and clouds, *J. Geophys. Res.*, *113*, D02203, doi:10.1029/2007JD008434.
King, M. D., W. P. Menzel, Y. J. Kaufman, D. Tanre, B. C. Gao, S. Platnick, S. A. Ackerman, L. A. Remer, R. Pincus, and P. A. Hubanks (2003), Cloud and aerosol properties, precipitable water, and profiles of temperature and water vapor from MODIS, *IEEE Trans. Geosci. Remote Sens.*, *41*, 442–458.
Koehler, K. A., P. J. DeMott, S. M. Kreidenweis, O. B. Popovicheva, M. D. Petters, C. M. Carrico, E. D. Kireeva, T. D. Khokhlova, and N. K. Shonija (2009), Cloud condensation nuclei and ice nucleation activity of hydrophobic and hydrophilic soot particles, *Phys. Chem. Chem. Phys.*, *11*, 7906–7920.
Koehler, K. A., S. M. Kreidenweis, P. J. DeMott, M. D. Petters, A. J. Prenni, and O. Möhler (2010), Laboratory investigations of the impact of mineral dust aerosol on cold cloud formation, *Atmos. Chem. Phys.*, *10*, 11,955–11,968.
Koop, T., B. P. Luo, A. Tsias, and T. Peter (2000), Water activity as the determinant for homogeneous ice nucleation in aqueous solutions, *Nature*, *406*, 611–614.
Krämer, M., et al. (2009), Ice supersaturations and cirrus cloud crystal numbers, *Atmos. Chem. Phys.*, *9*, 3505–3522.
Lawson, R. P., B. Pilson, B. Baker, Q. Mo, E. Jensen, L. Pfister, and P. Bui (2008), Aircraft measurements of microphysical properties of subvisible cirrus in the tropical tropopause layer, *Atmos. Chem. Phys.*, *8*, 1609–1620.
Lee, D. S., D. W. Fahey, P. M. Forster, P. J. Newton, R. C. N. Wit, L. L. Lim, B. Owen, and R. Sausen (2009), Aviation and global climate change in the 21st century, *Atmos. Environ.*, *43*, 3520–3537.
Levkov, L., B. Rockel, H. Kapitza, and E. Raschke (1992), 3D mesoscale numerical studies of cirrus and stratus clouds by their time and space evolution, *Beitr. Phys. Atmos.*, *65*, 35–58.
Liu, X., and J. E. Penner (2005), Ice nucleation parameterization for global models, *Meteorol. Z.*, *14*, 499–514.
Liu, X., J. E. Penner, S. Ghan, and M. Wang (2007), Inclusion of ice microphysics in the NCAR Community Atmospheric Model version 3 (CAM3), *J. Clim.*, *20*, 4526–4547.
Liu, X., J. E. Penner, and M. Wang (2009), Influence of anthropogenic sulfate and black carbon on upper tropospheric clouds in the NCAR CAM3 model coupled to the IMPACT global aerosol model, *J. Geophys. Res.*, *114*, D03204, doi:10.1029/2008JD010492.
Lohmann, U. (2002), Possible aerosol effects on ice clouds via contact nucleation, *J. Atmos. Sci.*, *59*, 647–656.
Lohmann, U., and J. Feichter (2005), Global indirect aerosol effects: A review, *Atmos. Chem. Phys.*, *5*, 715–737.
Lohmann, U., and B. Kärcher (2002), First interactive simulations of cirrus clouds formed by homogeneous freezing in the ECHAM GCM, *J. Geophys. Res.*, *107*(D10), 4105, doi:10.1029/2001JD000767.
Lohmann, U., and E. Roeckner (1996), Design and performance of a new cloud microphysics scheme developed for the ECHAM general circulation model, *Clim. Dyn.*, *12*, 557–572.
Lohmann, U., J. Feichter, C. C. Chuang, and J. E. Penner (1999), Predicting the number of cloud droplets in the ECHAM GCM, *J. Geophys. Res.*, *104*, 9169–9198.
Lohmann, U., B. Kärcher, and C. Timmreck (2003), Impact of the Mt. Pinatubo eruption on cirrus clouds formed by homogeneous freezing in the ECHAM GCM, *J. Geophys. Res.*, *108*(D18), 4568, doi:10.1029/2002JD003185.
Lohmann, U., B. Kärcher, and J. Hendricks (2004), Sensitivity studies of cirrus clouds formed by heterogeneous freezing in the ECHAM GCM, *J. Geophys. Res.*, *109*, D16204, doi:10.1029/2003JD004443.
Lohmann, U., P. Spichtinger, S. Jess, T. Peter, and H. Smit (2008), Cirrus cloud formation and ice supersaturated regions in a global climate model, *Environ. Res. Lett.*, *3*, 045022, doi:10.1088/1748-9326/3/4/045022.
McFarquhar, G. M., and A. J. Heymsfield (1997), Parameterization of tropical cirrus ice crystal size distributions and implications for radiative transfer: Results from CEPEX, *J. Atmos. Sci.*, *54*, 2187–2200.
McFarquhar, G. M., J. Um, M. Freer, D. Baumgardner, G. L. Kok, and G. Mace (2007), Importance of small ice crystals to cirrus properties: Observations from the Tropical Warm Pool International Cloud Experiment (TWP-ICE), *Geophys. Res. Lett.*, *34*, L13803, doi:10.1029/2007GL029865.
Meyers, M. P., P. J. DeMott, and W. R. Cotton (1992), New primary ice-nucleation parameterization in an explicit cloud model, *J. Appl. Meteorol.*, *31*, 708–721.
Minikin, A., A. Petzold, J. Ström, R. Krejci, M. Seifert, P. van Velthoven, H. Schlager, and U. Schumann (2003), Aircraft observations of the upper tropospheric fine particle aerosol in the Northern and Southern Hemispheres at midlatitudes, *Geophys. Res. Lett.*, *30*(10), 1503, doi:10.1029/2002GL016458.
Möhler, O., et al. (2005), Effect of sulfuric acid coating on heterogeneous ice nucleation by soot aerosol particles, *J. Geophys. Res.*, *110*, D11210, doi:10.1029/2004JD005169.
Möhler, O., et al. (2006), Efficiency of the deposition mode ice nucleation on mineral dust particles, *Atmos. Chem. Phys.*, *6*, 3007–3021.
Möhler, O., S. Benz, H. Saathoff, M. Schnaiter, R. Wagner, J. Schneider, S. Walter, V. Ebert, and S. Wagner (2008), The effect of organic coating on the heterogeneous ice nucleation efficiency of mineral dust aerosols, *Environ. Res. Lett.*, *3*, 025007, doi:10.1088/1748-9326/3/2/025007.
Murakami, M. (1990), Numerical modeling of dynamical and microphysical evolution of an isolated convective cloud—The 19 July 1981 CCOPE cloud, *J. Meteorol. Soc. Jpn.*, *68*, 107–128.
Murray, B. J. (2008), Inhibition of ice crystallisation in highly viscous aqueous organic acid droplets, *Atmos. Chem. Phys.*, *8*, 5423–5433.
Murray, B. J., et al. (2010), Heterogeneous nucleation of ice particles on glassy aerosols under cirrus conditions, *Nat. Geosci.*, *3*, 233–237.
Penner, J. E., Y. Chen, M. Wang, and X. Liu (2009), Possible influence of anthropogenic aerosols on cirrus clouds and anthropogenic forcing, *Atmos. Chem. Phys.*, *9*, 879–896.
Petzold, A., M. Fiebig, H. Flentje, A. Keil, U. Leiterer, F. Schröder, A. Stifter, M. Wendisch, and P. Wendling (2002), Vertical variability of aerosol properties observed at a continental site during the Lindenberg Aerosol Characterization Experiment (LACE 98), *J. Geophys. Res.*, *107*(D21), 8128, doi:10.1029/2001JD001043.
Rädel, G., C. J. Stubenrauch, R. Holz, and D. L. Mitchell (2003), Retrieval of effective ice crystal size in the infrared: Sensitivity study and global measurements from the TIROS-N operational vertical sounder, *J. Geophys. Res.*, *108*(D9), 4281, doi:10.1029/2002JD002801.
Roeckner, E., K. Arpe, L. Bengtsson, M. Christoph, M. Claussen, L. Dümenil, M. Esch, M. Giorgetta, U. Schlese, and U. Schulzweida (1996), The atmospheric general circulation model ECHAM4: Model description and simulation of the present day climate, *Tech. Rep. 218*, Max-Planck-Inst. für Meteorol., Hamburg, Germany.
Rogers, D. C., P. J. DeMott, S. M. Kreidenweis, and Y. Chen (1998), Measurements of ice nucleating aerosols during SUCCESS, *Geophys. Res. Lett.*, *25*, 1383–1386.
Rossow, W. B., and R. A. Schiffer (1999), Advances in understanding clouds from ISCCP, *Bull. Am. Meteorol. Soc.*, *80*, 2261–2287.
Salzmann, M., Y. Ming, J.-C. Golaz, P. A. Ginoux, H. Morrison, A. Gettelman, M. Krämer, and L. J. Donner (2010), Two-moment bulk stratiform cloud microphysics in the GFDL AM3 GCM: Description, evaluation, and sensitivity tests, *Atmos. Chem. Phys.*, *10*, 8037–8064.
Scott, N. A., A. Chédin, R. Armante, J. Francis, C. Stubenrauch, J. P. Chaboureau, F. Chevallier, C. Claud, and F. Chéruy (1999), Characteristics of the TOVS Pathfinder Path-B dataset, *Bull. Am. Meteorol. Soc.*, *80*, 2679–2701.
Sölch, I., and B. Kärcher (2011), Process-oriented large eddy simulations of a mid-latitude cirrus cloud system based on observations, *Q. J. R. Meteorol. Soc.*, *137*, 374–393.
Spichtinger, P., K. Gierens, and W. Read (2003), The global distribution of ice-supersaturated regions as seen by the Microwave Limb Sounder, *Q. J. R. Meteorol. Soc.*, *129*, 3391–3410.
Spichtinger, P., K. Gierens, H. G. J. Smit, J. Ovarlez, and J.-F. Gayet (2004), On the distribution of relative humidity in cirrus clouds, *Atmos. Chem. Phys.*, *4*, 639–647.
Stubenrauch, C. J., F. Eddounia, and G. Rädel (2004), Correlations between microphysical properties of large-scale semi-transparent cirrus and the state of the atmosphere, *Atmos. Res.*, *72*, 403–423.
Sundqvist, H., E. Berge, and J. E. Kristiansson (1989), Condensation and cloud parameterization studies with a mesoscale numerical weather prediction model, *Mon. Weather Rev.*, *117*, 1641–1657.
Susskind, J., P. Piraino, L. Rokke, T. Iredell, and A. Mehta (1997), Characteristics of the TOVS Pathfinder Path A dataset, *Bull. Am. Meteorol. Soc.*, *78*, 1449–1472.
Vali, G. (1985), Atmospheric ice nucleation—A review, *J. Rech. Atmos.*, *19*, 105–115.
Waliser, D., et al. (2009), Cloud ice: A climate model challenge with signs and expectations of progress, *J. Geophys. Res.*, *114*, D00A21, doi:10.1029/2008JD010015.
Wang, M., and J. E. Penner (2010), Cirrus clouds in a global climate model with a statistical cirrus cloud scheme, *Atmos. Chem. Phys.*, *10*, 5449–5474.
Waters, J. W., et al. (2006), The Earth Observing System Microwave Limb Sounder (EOS MLS) on the Aura satellite, *IEEE Trans. Geosci. Remote Sens.*, *44*, 1075–1092, doi:10.1109/TGRS.2006.873771.
Welti, A., F. Lüönd, O. Stetzer, and U. Lohmann (2009), Influence of particle size on the ice nucleating ability of mineral dusts, *Atmos. Chem. Phys.*, *9*, 6705–6715.

Wiacek, A., T. Peter, and U. Lohmann (2010), The potential influence of Asian and African mineral dust on ice, mixed-phase and liquid water clouds, *Atmos. Chem. Phys.*, *10*, 8649–8667.

Wise, M. E., K. J. Baustian, and M. A. Tolbert (2009), Laboratory studies of ice formation pathways from ammonium sulfate particles, *Atmos. Chem. Phys.*, *9*, 1639–1646.

Wu, D. L., J. H. Jiang, W. G. Read, R. T. Austin, C. P. Davis, A. Lambert, G. L. Stephens, D. G. Vane, and J. W. Waters (2008), Validation of the Aura MLS cloud ice water content measurements, *J. Geophys. Res.*, *113*, D15S10, doi:10.1029/2007JD008931.

Zhang, Y., A. Macke, and F. Albers (1999), Effect of crystal size spectrum and crystal shape on stratiform cirrus radiative forcing, *Atmos. Res.*, *52*, 59–75.

Zuberi, B., A. K. Bertram, C. A. Cassa, L. T. Molina, and M. J. Molina (2002), Heterogeneous nucleation of ice in $(NH_4)_2SO_4$-H_2O particles with mineral dust immersions, *Geophys. Res. Lett.*, *29*(10), 1504, doi:10.1029/2001GL014289.

J. Hendricks and B. Kärcher, Deutsches Zentrum für Luft- und Raumfahrt, Institut für Physik der Atmosphäre, Oberpfaffenhofen, D-82234 Wessling, Germany. (johannes.hendricks@dlr.de)

U. Lohmann, Institut für Atmosphäre und Klima, ETH Zürich, Universitätstrasse 16, CH-8092 Zürich, Switzerland.